

# Dynamics of KPI lumps

Sarbarish Chakravarty and Michael Zowada

*Department of Mathematics, University of Colorado, Colorado Springs, CO 80918*

## Abstract

A family of nonsingular rational solutions of the Kadomtsev-Petviashvili (KP) I equation are investigated. These solutions have multiple peaks whose heights are time-dependent and the peak trajectories in the  $xy$ -plane are altered after collision. Thus they differ from the standard multi-peaked KPI simple  $n$ -lump solutions whose peak heights as well as peak trajectories remain unchanged after interaction. The anomalous scattering occurs due to a non-trivial internal dynamics among the peaks in a slow time scale. This phenomena is explained by relating the peak locations to the roots of complex heat polynomials. It follows from the long time asymptotics of the solutions that the peak trajectories separate as  $O(\sqrt{|t|})$  as  $|t| \rightarrow \infty$ , and all the peak heights approach the same constant value corresponding to that of the simple 1-lump solution. Consequently, a multi-peaked  $n$ -lump solution evolves to a superposition of  $n$  1-lump solutions asymptotically as  $|t| \rightarrow \infty$ .

## 1 Introduction

Many nonlinear wave equations admit special classes of exact solutions in the form of solitary waves that are of physical interest. Such equations arise in such diverse fields as fluid dynamics, nonlinear optics, magnetic systems, and plasma physics. An important example of such special nonlinear wave equations is the Kadomtsev-Petviashvili (KP) equation, which is a  $(2+1)$ -dimensional dispersive equation describing the propagation of small amplitude, long wavelength, uni-directional waves with small transverse variation (i.e., quasi-two-dimensional waves). It was originally proposed by Kadomtsev and Petviashvili [20] and has found applications in the study of ion-acoustic (see e.g. [18, 23] and references therein), and shallow water waves (see e.g. the monographs [1, 6, 21]). The KP equation is also an integrable nonlinear equation with remarkably rich mathematical structure which are documented in many research monographs (see e.g. [1, 27, 2, 18, 17, 21]).

There are two mathematically distinct versions of the KP equation, referred to as KPI and KP II. This article is concerned with the KPI equation which can be expressed as

$$(4u_t + 6uu_x + u_{xxx})_x = 3u_{yy}. \quad (1.1)$$

Here  $u = u(x, y, t)$  represents the normalized wave amplitude at the point  $(x, y)$  in the  $xy$ -plane for fixed time  $t$ , and the subscripts denote partial derivatives. Switching  $3u_{yy}$  to  $-3u_{yy}$  in (1.1) yields the KP II equation. From the water wave theory perspective, KPI corresponds to large surface tension while KP II arises in the small surface tension limit of the multiple-scale asymptotics [1, 6].

The KPI equation admits large classes of exact rational solutions known as lumps which are localized in the  $xy$ -plane and are non-singular for all  $t$ . The simplest type of rational solutions was first discovered analytically by employing the dressing method [24] and subsequently via the Hirota method [35]. These simple  $n$ -lump solutions consist of  $n$  peaks which interact without any change of form or phase. Each peak travels with distinct asymptotic velocity and its trajectory remains unchanged before and after interaction as  $|t| \rightarrow \infty$ . These solutions were also obtained via the inverse scattering transform (IST) in [15] where it was shown that the simple lumps (for a fixed  $t$ ) correspond to bound state potentials associated with complex conjugate pairs of simple eigenvalues of the non-stationary Schrödinger equation. Yet another class of KPI rational solutions arise as bound states corresponding to eigenvalues with multiplicities associated with the time-dependent Schrödinger equation, and are also amenable to IST methodology [3, 39]. These are called the multi-lump solutions which were originally found in [19] by algebraic techniques and further investigated by several authors [29, 16, 4]. The multi-lump solution is an

ensemble of a finite number of localized structures (or peaks) interacting in a non-trivial manner unlike the  $n$ -simple lump solution. The peaks move with the same center-of-mass velocity but undergo anomalous scattering with a non-zero deflection angle after collision. Furthermore, the peak amplitudes evolve in time and reaches a constant asymptotic value which equals that of the simple 1-lump peak. It has been also known [22, 16, 36] that the dynamics of the KPI lumps are related to the multi-particle Calogero-Moser system; this connection was further explored in [30, 31].

The purpose of this article is to revisit a special family of multi-lump solutions referred throughout the article as the  $n$ -lump solutions which are relatively simple to construct. We carry out a detailed study of their dynamics, which, to the best of our knowledge, was not done earlier. The family of solutions considered here exhibit a simple yet interesting interaction pattern, namely, that in a comoving frame the multiple lumps interact along a line and move away from each other along an orthogonal line in the plane after the interaction process is complete. Such anomalous scattering process is different from the usual scattering of KP solitons or even the simple  $n$ -lump solutions. The comoving frame travels with a uniform velocity in the  $xy$ -plane, while the internal dynamics of the component lumps takes place at a slower time that scales as  $O(|t|^{1/2})$ . The anomalous scattering is explained by analyzing the explicit formulas for the simpler solutions and then via asymptotic analysis for the general case. The long-time asymptotics of the solutions are also worked out in order to demonstrate that indeed the solution splits up into  $n$  distinct peaks like it is usually assumed in the literature. The peak locations evolve as a dynamical system which is a reduction of the Calogero-Moser system, and can be related to the zeros of polynomial solutions of the complex two-dimensional heat equation. An elementary analysis of the dynamical system provides a simple analytical explanation of the anomalous (90-degree) scattering of the  $n$ -lump solutions. Finally, the eigenfunction of the KP Lax pair associated with the  $n$ -lump solutions are derived via binary Darboux transformations to make connection with the results obtained by the IST method. The binary Darboux transformation yields simple explicit formula for the  $n$ -lump eigenfunction that is rather difficult to obtain from the IST method. Although some topics of this article had been investigated in the past by several authors (including one of the present authors), we believe that the explicit formulas for the polynomial  $\tau$ -function and the  $n$ -lump eigenfunction, along with the long time asymptotics developed to study the peak dynamics in terms of heat polynomials, are some of the new results obtained in this paper.

The paper is structured as follows: in Section 2 the generalized Schur polynomials are introduced; these polynomials play a fundamental role in the theory of rational, multi-lump solutions of KPI. Then a polynomial form of the  $n$ -lump  $\tau$ -function is constructed in terms of these polynomials. Some examples of solutions for  $n = 1, 2, 3$  are discussed in Section 3. Section 4 is devoted to the asymptotic analysis of the  $n$ -lump solution for large  $|t|$  and the connection to the complex heat polynomials in two-dimension. The binary Darboux transformation and its application to construct the eigenfunction for the Lax pair associated with the  $n$ -lump solution and connection with some results obtained via IST are presented in Section 5. Section 6 contains some concluding remarks including future directions of this continued investigation of KPI lumps. Finally, an appendix validating the approximation used throughout Sections 3 and 4 to estimate the exact locations of the  $n$ -lump peaks, is included.

## 2 Construction of special multi-lumps

In this section we describe how to construct a special class of the multi-lump solutions in a straight-forward, algebraic fashion. Although this construction is related to the binary Darboux transformation or the so called Grammian technique, no prior knowledge of such methods is required for this particular case. The building blocks for these solutions are given by a special type of complex polynomials called the generalized Schur polynomials which are introduced below.

## 2.1 Generalized Schur polynomials

Let  $k$  be a complex parameter and  $\theta := kx + k^2y + k^3t + \gamma(k)$  where  $(x, y, t) \in \mathbb{R}^3$  and  $\gamma(k)$  is an arbitrary function which is differentiable to all orders. Then the generalized Schur polynomial  $p_n$  is defined via the relation

$$\phi_n := \frac{1}{n!} \partial_k^n \exp(i\theta) = p_n \exp(i\theta). \quad (2.1)$$

It is easy to see that  $p_n = p_n(\theta_1, \theta_2, \dots, \theta_n)$  where  $\theta_j := i\partial_k^j \theta / j!$ . However, only the first three

$$\theta_1 = i(x + 2ky + 3k^2t + \gamma_1), \quad \theta_2 = i(y + 3kt + \gamma_2), \quad \theta_3 = i(t + \gamma_3) \quad (2.2)$$

depend on  $(x, y, t)$  while  $\theta_j = i\gamma_j$  for  $j > 3$ . Here,  $\gamma_j(k) = \partial_k^j \gamma(k) / j!$ ,  $j = 1, \dots, n$  are to be viewed as independent complex parameters depending on the  $k$ -derivatives of  $\gamma(k)$ . A generating function for the  $p_n$ 's is given by the Taylor series

$$\exp(i\theta(k+h)) = \exp(i\theta) \sum_{n=0}^{\infty} p_n(k) h^n, \quad (2.3)$$

which yields, after expanding  $i\theta(k+h) = i\theta(k) + h\theta_1 + h^2\theta_2 + \dots$ , and comparing with the right hand side, an explicit expression for  $p_n$ , namely

$$p_n = \sum_{\substack{m_1, m_2, \dots, m_n \geq 0 \\ m_1 + 2m_2 + \dots + nm_n = n}} \prod_{j=1}^n \frac{\theta_j^{m_j}}{m_j!}. \quad (2.4)$$

The first few generalized Schur polynomials are given by

$$p_0 = 1, \quad p_1 = \theta_1, \quad p_2 = \frac{1}{2}\theta_1^2 + \theta_2, \quad p_3 = \frac{1}{3!}\theta_1^3 + \theta_1\theta_2 + \theta_3 \dots$$

It follows from (2.4) that the  $p_n$  is a *weighted* homogeneous polynomial of degree  $n$  in  $\theta_j$ ,  $j = 1, \dots, n$ , i.e.,  $p_n(a\theta_1, a^2\theta_2, \dots, a^n\theta_n) = a^n p_n(\theta_1, \theta_2, \dots, \theta_n)$ , where  $\text{weight}(\theta_j) = j$ . Some useful properties including recurrence relations for the  $p_n$ 's can be derived using (2.1) and (2.3). These are listed below and will be used throughout this article.

$$\partial_{\theta_1}^j p_n = \partial_{\theta_j} p_n = \begin{cases} p_{n-j}, & j \leq n \\ 0, & j > n \end{cases} \quad (2.5a)$$

$$p_{n+1}(k) = \frac{1}{n+1} \sum_{j=0}^n (j+1) \theta_{j+1} p_{n-j}, \quad n \geq 0, \quad p_0 = 1 \quad (2.5b)$$

$$p_n(\theta_1 + h_1, \theta_2 + h_2, \dots, \theta_n + h_n) = \sum_{j=0}^n p_j(h_1, h_2, \dots, h_j) p_{n-j}(\theta_1, \theta_2, \dots, \theta_{n-j}) \quad (2.5c)$$

### Remarks

- (a) The generalized Schur polynomials were used earlier in the study of rational solutions for the Zakharov-Shabat and KP hierarchies [25, 30, 31]. These involve multi-time variables with the phase defined as quasi-polynomial  $\theta = kt_1 + k^2t_2 + k^3t_3 + \dots$ . In this paper, we restrict the  $p_n$ 's to depend only on the first three variables  $(t_1, t_2, t_3) = (x, y, t)$  while the dependence on the remaining variables are parametric, through the complex parameters  $\theta_j = i\gamma_j$  for  $j > 3$ .
- (b) By choosing  $\theta$  instead of  $i\theta$  where  $\theta = kt_1 + k^2t_2 + k^3t_3 + \dots$  depends on infinitely many "time" variables, and by evaluating the  $k$ -derivatives at  $k = 0$  in (2.1), one recovers the standard Schur polynomials which play an important role in the Sato theory of the KP hierarchy [34] (see also [28, 21]). In fact, then the Schur polynomials are generated by (2.3) with  $k = 0$  (and  $i\theta \rightarrow \theta$ ), and are given explicitly by the formula (2.4) with  $\theta_j \rightarrow t_j$ .

## 2.2 The multi-lump $\tau$ -function

The solution of the KPI equation (1.1) can be expressed as

$$u(x, y, t) = 2(\ln \tau)_{xx}, \quad (2.6)$$

where the function  $\tau(x, y, t)$  is known as the  $\tau$ -function [34, 17]. Here we describe how to construct a polynomial  $\tau$ -function which yields a special family of rational multi-lump solutions of KPI.

First, we note that the exponential  $\exp(i\theta)$  introduced in Section 2.1 as well as its  $k$ -derivative of any order, solve the linear system

$$i\phi_y = \phi_{xx}, \quad \phi_t + \phi_{xxx} = 0, \quad (2.7)$$

where  $\phi(x, y, t, k)$  is parametrized by  $k \in \mathbb{C}$ . Next we take  $\phi_n(x, y, t, k) = p_n \exp(i\theta)$  as given in (2.1) and its complex conjugate  $\bar{\phi}_n$  to define a  $n$ -lump  $\tau$ -function as follows:

$$\tau_n(x, y, t) = \int_x^\infty \phi_n \bar{\phi}_n dx' = \int_x^\infty |p_n|^2 \exp i(\theta - \bar{\theta}) dx', \quad (2.8)$$

where the parameter  $k$  in  $\theta = kx + k^2y + k^3t + \theta_0(k)$  is chosen such that  $b := \text{Im}(k) > 0$  in order for the integral above to converge. The integral in (2.8) may be evaluated by integration by parts, then from (2.6), the  $n$ -lump solution is given by

$$u_n(x, y, t) = 2(\ln \tau_n)_{xx} = 2(\ln F_n)_{xx}, \quad F_n = \sum_{j=0}^{2n} \frac{\partial_x^j |p_n|^2}{(2b)^j}, \quad (2.9)$$

where the last equality follows since the factor  $\frac{1}{2b} \exp i(\theta - \bar{\theta})$  in  $\tau_n$  is annihilated by  $\ln(\cdot)_{xx}$ . Recall from Section 2.1 that  $p_n$  is a polynomial of degree  $n$  in  $x, y, t$ , hence  $F_n$  is a polynomial of degree  $2n$  in  $x, y, t$ . Consequently,  $u_n(x, y, t)$  is a rational function of its arguments and decays as  $\frac{1}{R^2}$  as  $R = \sqrt{x^2 + y^2} \rightarrow \infty$  for fixed  $t$ .

It can be directly shown that the  $\tau_n$  in (2.8) is indeed a  $\tau$ -function for the KPI equation. Inserting (2.6) into (1.1), integrating the resulting equation twice with respect to  $x$ , and setting the integration constants to zero (since for lumps, the derivatives of  $\ln(\tau)$  vanish as  $R \rightarrow \infty$ ), one obtains

$$4(\tau\tau_{xt} - \tau_x\tau_t) - 3\tau_{xx}^2 - \tau\tau_{xxxx} + 4\tau_x\tau_{xxx} - 3\tau_y^2 + 3\tau\tau_{yy} = 0.$$

Next, by setting  $\tau = \tau_n$  from (2.8) in the above equation, and using (2.7) and its complex conjugate with  $\phi = \phi_n$ , a straight-forward calculation yields the desired result.

It is evident from (2.9) that the multi-lump solution is in effect determined by the polynomial part of  $\tau_n$ , namely,  $F_n(x, y, t)$ . The expression for  $F_n$  in (2.9) can be cast as a Hermitian form as follows:

$$\begin{aligned} F_n(x, y, t) &= \sum_{j=0}^{2n} \frac{1}{(2b)^j} \sum_{l=0}^j \binom{j}{l} \partial_x^l p_n \partial_x^{j-l} \bar{p}_n = \sum_{l=0}^n \sum_{m=0}^n \frac{1}{(2b)^{l+m}} \binom{l+m}{m} \partial_x^l p_n \partial_x^m \bar{p}_n \\ &= p^\dagger C p, \quad \text{with } p = (p_n, \partial_x p_n, \dots, \partial_x^n p_n), \quad C_{lm} = \frac{1}{(2b)^{l+m}} \binom{l+m}{m}, \end{aligned}$$

and where  $C$  is a real, symmetric  $(n+1) \times (n+1)$  matrix. The matrix  $C$  admits a unique decomposition  $C = U^\dagger D U$  where  $U$  is a real, upper-triangular matrix with 1's along its main diagonal and  $D$  is a diagonal matrix with  $D_{jj} = (2b)^{-2j}$ ,  $j = 0, 1, \dots, n$ . Hence,  $F_n$  can be expressed as a sum of squares  $F_n = q^\dagger D q$ ,  $q = U p$ , which can be explicitly written as

$$F_n(x, y, t) = \sum_{j=0}^n \left| \sum_{l=j}^n \binom{l}{j} \frac{\partial_x^l p_n}{(2b)^l} \right|^2 = \sum_{j=0}^n \left| \sum_{l=j}^n \binom{l}{j} \left( \frac{i}{2b} \right)^l p_{n-l} \right|^2, \quad (2.10)$$

the last equality uses the fact  $\partial_x p_n = i\partial_{\theta_1} p_n = ip_{n-1}$ , which follows from (2.2) and (2.5a). It should be clear from the expression of the generalized Schur polynomials in (2.4) and the definitions of the  $\theta_1, \theta_2, \theta_3$  in (2.2) that  $F_n$  in (2.10) is a positive definite polynomial in  $x, y, t$  of degree  $2n$ , and it depends on  $2n + 2$  real parameters, namely,  $k := a + ib$  and  $\gamma_j \in \mathbb{C}$ ,  $j = 1, 2, \dots, n$ . Moreover,  $F_n$  is also a weighted homogeneous polynomial of degree  $2n$  in  $\theta_j, \bar{\theta}_j$   $j = 1, 2, \dots, n$  and  $\text{Im}(k) = b$  with  $\text{weight}(\theta_j) = \text{weight}(\bar{\theta}_j) = j$ , and  $\text{weight}(b) = -1$ . Consequently, the KPI multi-lump solution  $u_n(x, y, t)$  given by (2.9) is a non-singular, rational function in the  $xy$ -plane for all values of  $t$ .

### Remarks

- (a) One could exploit the linearity of the system (2.7) to choose

$$\phi_n = \sum_{j=0}^n a_j(k) p_j(\theta_1, \dots, \theta_j) \exp(i\theta(k))$$

instead, to construct the  $\tau$ -function in (2.8). However, the above sum can be reduced to a single generalized Schur polynomial  $p_n(\theta_1 + h_1, \dots, \theta_n + h_n)$  using (2.5c) for suitable choices for the  $h_j$ 's which can then be absorbed in the arbitrary constants  $\gamma_j$  appearing in the  $\theta_j$  variables for  $j = 1, \dots, n$ .

- (b) The function  $\phi_n = p_n \exp(i\theta)$  is also a  $\tau$ -function for the KPI equation. But the corresponding rational solution  $u(x, y, t)$  given by (2.6) is singular in the  $xy$ -plane for any given  $t$ . The singularities occur at the zeros of the generalized Schur polynomial  $p_n$ .
- (c) Since the KPI equation admits a constant solution  $u(x, y, t) = c$ ,  $c \in \mathbb{R}$ , one may be interested in studying the multi-lump solutions in a constant background. This is easily accomplished by a few small modifications as follows: Equation (2.9) should read as  $u_n = c + 2(\ln \tau_n)_{xx}$  where  $\tau_n$  is given by (2.8) except that the  $\phi_n$  satisfies the linear system:  $i\phi_y = \phi_{xx} + c\phi$ ,  $\phi_t + \phi_{xxx} + \frac{3}{4}c\phi_x = 0$ . The solution to this new linear system is given by  $\phi_n = \frac{1}{n!} \partial_k^n \exp(i\theta') = p'_n \exp(i\theta')$  where  $\theta' = kx + (k^2 - c)y + (k^3 - \frac{3}{4}kc)t + \gamma(k)$ . The new generalized Schur polynomials  $p'_n$  are defined in the same way as before, the only change being  $x \rightarrow x - \frac{3}{4}ct$  in the definition of  $\theta_1$  in (2.2).
- (d) Several authors [13, 10] have considered a more general choice for  $\phi_n$  such as  $\phi_n = D_k^n \exp(i\theta)$  with  $\theta(k)$  same as before but  $D_k := f(k)\partial_k$  where  $f(k)$  is analytic. In such cases, it is possible to consider  $D_k = \partial_z$  in terms of a (local) uniformizing variable  $z(k)$  with  $z'(k) = 1/f(k)$  and an appropriate branch of its inverse  $k(z)$  to express  $\theta(k(z))$ . Thus this approach is consistent with this section's formalism although the corresponding rational KPI solutions are different due to differing choices for the generalized Schur polynomials  $p_n(z)$ .

## 3 Examples of multi-lump solutions

We now give some examples of the KPI multi-lump solutions and illustrate the interaction properties of such solutions. It will be convenient to first introduce a set of coordinates  $r, s$  defined in terms of co-moving coordinates  $x', y'$  as follows

$$r = x' + 2ay', \quad s = 2by', \quad \text{where} \quad x' = x - 3(a^2 + b^2)t, \quad y' = y + 3at, \quad (3.1)$$

and recall that  $a = \text{Re}(k)$ ,  $b = \text{Im}(k)$ . As will be shown below that  $r, s$  are the natural coordinates to use instead of the  $x, y$ . The  $\theta_j$  variables defined in (2.2) are then given by

$$\theta_1 = i(r + is + \gamma_1), \quad \theta_2 = \frac{is}{2b} - 3bt + i\gamma_2, \quad \theta_3 = i(t + \gamma_3) \quad (3.2)$$

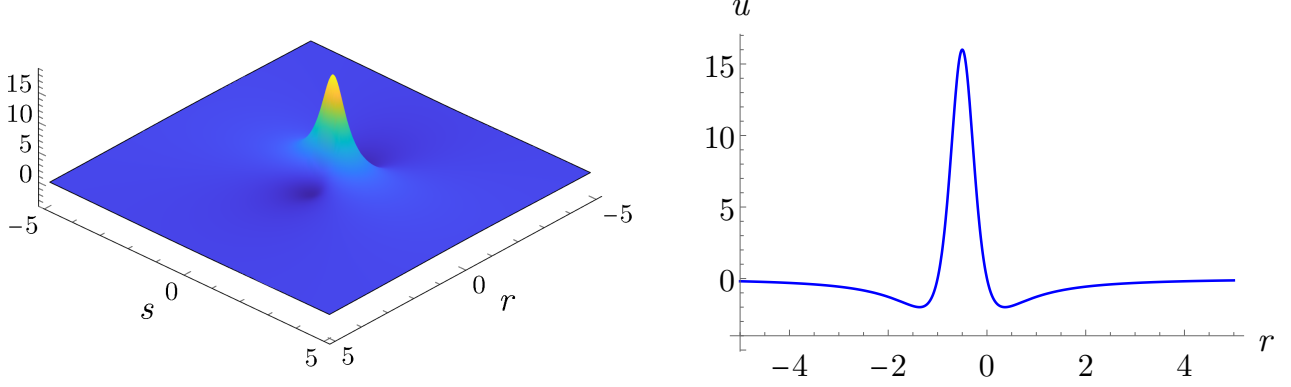


Figure 1: 1-lump solution of the KPI equation:  $a = \gamma_1 = 0, b = 1$ . Right: Vertical crosssection showing the maximum and two minima.

### 3.1 1-lump solution

For  $n = 1$ , the polynomial  $F_1$  is obtained from (2.10) after using  $p_0 = 1, p_1 = \theta_1$  as

$$F_1 = |\theta_1 + \frac{i}{2b}|^2 + \frac{1}{4b^2} = (r + \frac{1}{2b} - r_0)^2 + (s - s_0)^2 + \frac{1}{4b^2}, \quad r_0 = \text{Re}(\gamma_1), \quad s_0 = \text{Im}(\gamma_1),$$

where (3.2) is used to obtain the second expression of  $F_1$ . Then from (2.9), the 1-lump solution is given by

$$u_1(x, y, t) = 2(\ln F_1)_{xx} = 4 \frac{-(r + \frac{1}{2b} - r_0)^2 + (s - s_0)^2 + \frac{1}{4b^2}}{[(r + \frac{1}{2b} - r_0)^2 + (s - s_0)^2 + \frac{1}{4b^2}]^2}. \quad (3.3)$$

Notice that the solution is *stationary* in the  $rs$ -plane since the only time dependence enters via the comoving coordinates  $x', y'$ . Hence, the 1-lump is a rational traveling wave with a single peak (maximum) at  $(r_0 - \frac{1}{2b}, s_0)$  of height  $16b^2$  and two local minima symmetrically located from the peak at  $(r_0 - \frac{1}{2b} \pm \frac{\sqrt{3}}{2b})$  and depth  $-2b^2$  determined by  $b$  and the complex parameter  $\gamma_1$  as illustrated in Figure 1. The wave moves in the  $xy$ -plane with a uniform velocity  $(3(a^2 + b^2), -3a)$  at an angle  $\tan^{-1}(-a/(a^2 + b^2))$  with the positive  $x$ -axis. Since  $u_1$  is the  $x$ -derivative of the rational function  $F_{1x}/F_1$  which decays as  $|x| \rightarrow \infty$  for all  $y, t$ , one has that  $\int_{-\infty}^{\infty} u_1 dx = 0$ . However, in the  $xy$ -plane  $u_1$  is not integrable in the Fubini-Tonelli sense. Hence,  $u_1$  is not a  $L^1(\mathbb{R}^2)$  function although  $u_1 \in L^2(\mathbb{R}^2)$  and  $\iint_{\mathbb{R}^2} u_1^2 = 16\pi b$ ; the latter is a conserved quantity for the KPI equation (1.1).

### 3.2 2-lump solution

In this case the polynomial  $F_2$  from (2.10) is given by

$$F_2 = |\frac{1}{2}((r + \frac{1}{2b})^2 - s^2) + 3bt + \frac{1}{8b^2} + irs|^2 + \frac{1}{4b^2}|(r + \frac{1}{b}) + is|^2 + \frac{1}{16b^4}, \quad (3.4)$$

where we have set the constants  $\gamma_1 = \gamma_2 = 0$  for simplicity. Notice that unlike  $F_1$ , the polynomial  $F_2(r, s, t)$  does depend explicitly on  $t$  so that the solution  $u_2$  obtained from (2.9) is non-stationary in the comoving  $rs$ -plane. The explicit expression for  $u_2(x, y, t)$  is complicated, so it is not included here. Figure 2 illustrates that  $u_2$  consists of 2 localized lumps along the  $r$ -axis that are well separated as  $t \ll 0$ ; these lumps get attracted to each other and overlap when  $t$  is finite, then separate when  $t \gg 0$  but along the  $s$ -axis. Furthermore, the height of each peak also evolve with time and approaches the constant height of the 1-lump solution as  $|t| \rightarrow \infty$ . The interaction process is an example of anomalous (inelastic) scattering rather than the usual solitonic interaction of the simple  $n$ -lump solution of KPI. In order to analyze the 2-lump interaction, the peak locations and heights need to be determined from the local maxima of the function  $u_2(x, y, t)$  but the necessary calculation is too complicated to yield exact

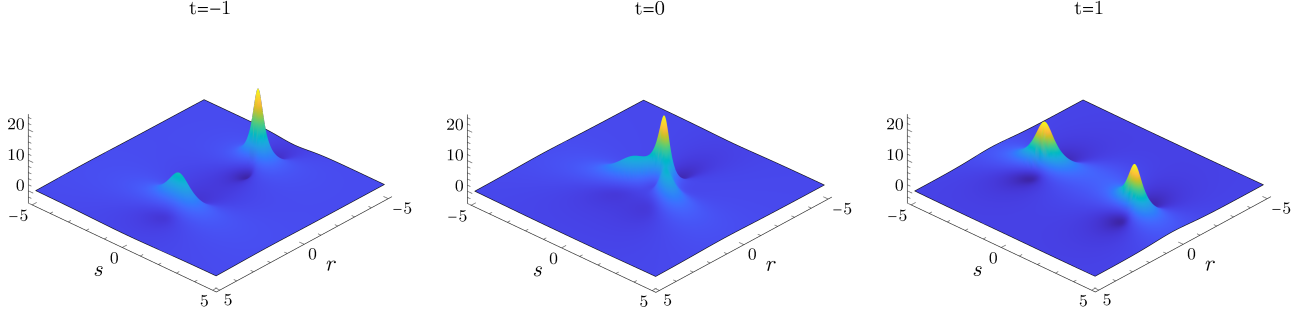


Figure 2: 2-lump solution of the KPI equation:  $a = \gamma_1 = \gamma_2 = 0, b = 1$ .

analytical formulas. Instead, we make certain approximations to estimate the leading order expressions for peak locations and heights. First, we note that the expression

$$u = 2 \ln(F)_{xx} = 2 \frac{F F_{xx} - F_x^2}{F^2}$$

for the solution suggests that the maximum for  $u_2$  occurs approximately near the minimum of the positive polynomial  $F_2$ . Secondly, the local minima of  $F_2$  are approximately located near the zeros of the leading order polynomial  $F_2^{(0)}$  which is the first of the three  $|\cdot|^2$  terms in (3.4) corresponding to the  $j = 0$ -term in (2.10). This assumption, which will be justified below (see also Appendix), makes the analytical computations tractable and corroborates the interaction process depicted in Figure 2 above. Setting  $F_2^{(0)} = 0$  and after solving for  $r$  and  $s$ , one obtains the approximate peak locations

$$(r_p, s_p) = \left(-\frac{1}{2b} \pm \sqrt{6b|t| - \frac{1}{4b^2}}, 0\right), \quad t \ll 0, \quad (r_p, s_p) = \left(0, \pm \sqrt{6bt + \frac{1}{2b^2}}\right), \quad t \gg 0. \quad (3.5)$$

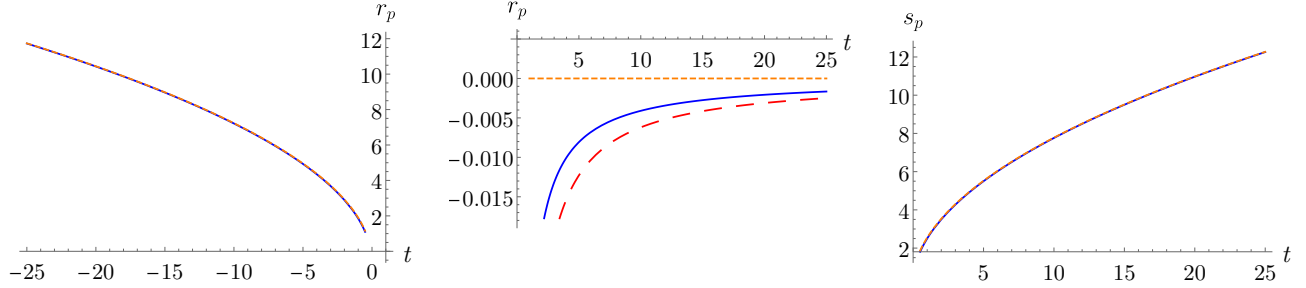


Figure 3: 2-lump peak locations. Exact (blue curve), approximate from (3.5) (orange dashed curve). Left panel:  $r_p(t)$  for right peak ( $s_p = 0$ ). Reflecting across the line  $r_p = -\frac{1}{2b}$  gives the left peak location. Middle panel:  $r_p(t)$  for top & bottom peak, red-dashed line corresponds to minimum of  $F_2$ . Right panel:  $s_p(t)$  for top peak, reflecting across  $t$ -axis gives  $s_p(t)$  of the bottom peak. KP parameters:  $a = \gamma_1 = \gamma_2 = 0, b = 1$ .

Equation (3.5) shows that the peaks are well-separated for  $|t| \gg 0$  and verifies the anomalous interaction process described above. It is also evident from (3.5) that the relative rates of attraction (along  $r$ -axis) and repulsion (along  $s$ -axis) is  $\sqrt{6b}|t|^{-1/2}$  as  $|t| \rightarrow \infty$ . The exact and approximate peak locations from (3.5) are almost indistinguishable as shown in Figure 3 which illustrates the accuracy of (3.5) for large  $t$ . The exact and approximate values differ by  $O(|t|^{-1/2})$  as will be shown below (and in the Appendix for the general  $n$ -lump solutions). This fact is manifested in the middle panel of Figure 3 which shows that the approximate value of  $r_p(t)$  for  $t \gg 0$ , obtained by minimizing  $F_2$  gives a better approximation  $r_p(t) = -\frac{1}{16b^4} \frac{1}{t} + O(t^{-2})$  than  $r_p(t) = 0$  given by (3.5). The difference between the two approximations is  $O(t^{-1})$ . From (3.1), the peak locations in the  $xy$ -plane are given by  $(x_p(t), y_p(t)) = (r_p(t) - 3(a^2 + b^2)|t|, 3a|t|)$  when  $t \ll 0$ , and the

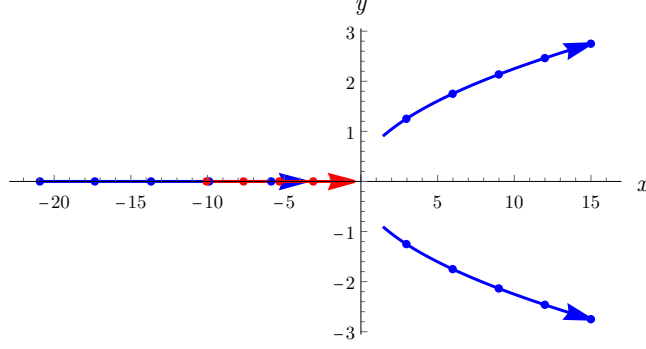


Figure 4: 2-lump peak trajectories in the  $xy$ -plane with  $a = 0$ . For  $t \ll 0$ , the trajectories degenerate along the negative  $x$ -axis with the blue dots indicating the faster peak. For  $t \gg 0$ , the parabolic trajectories are shown on the right-half  $xy$ -plane.

corresponding trajectory is a parabola which degenerates to the  $x$ -axis when the parameter  $a = 0$ . For  $t \gg 0$ ,  $(x_p(t), y_p(t)) = (3(a^2 + b^2)t - \frac{a}{b}s_p(t), -3at + \frac{s_p(t)}{2b})$ , and the trajectory is again a parabola in the  $xy$ -plane. If  $a = b$ , this parabola degenerates to a straight line  $x + 2ay = 0$ ,  $a \neq 0$ . A plot of a 2-lump trajectory in the  $xy$ -plane for  $a = 0$  is given in Figure 4.

The approximate peak heights can be calculated from the formula  $u_2(r_p, s_p)$  but since we assume that  $F$  attains its minimum value near  $(r_p, s_p)$ , we can take  $u_2 \approx 2F_{2xx}/F_2$ . Using (3.4) and (3.5), we obtain the following expressions for the approximate peak heights

$$u_{2p}^{\pm} = \frac{16b^2}{1 + \epsilon \pm 2\sqrt{\epsilon - \epsilon^2}}, \quad t \ll 0, \quad u_{2p} = 16b^2 - \frac{48b^2\epsilon}{1 + 7\epsilon}, \quad t \gg 0, \quad (3.6)$$

where  $\epsilon := (24b^3|t|)^{-1}$  and  $u_{2p}^-, u_{2p}^+$  denote the left and right peak heights, respectively. The peak heights approaches the 1-lump peak height  $16b^2$  asymptotically as  $|t| \rightarrow \infty$ . For  $t \ll 0$ , as the lumps approach each other along the  $r$ -axis, the left peak grows while the right peak decreases with time. But when  $t \gg 0$ , both peaks  $u_{2p}$  have the same value which increases with time and approaches the value  $16b^2$ . These features are illustrated by Figure 5 below.

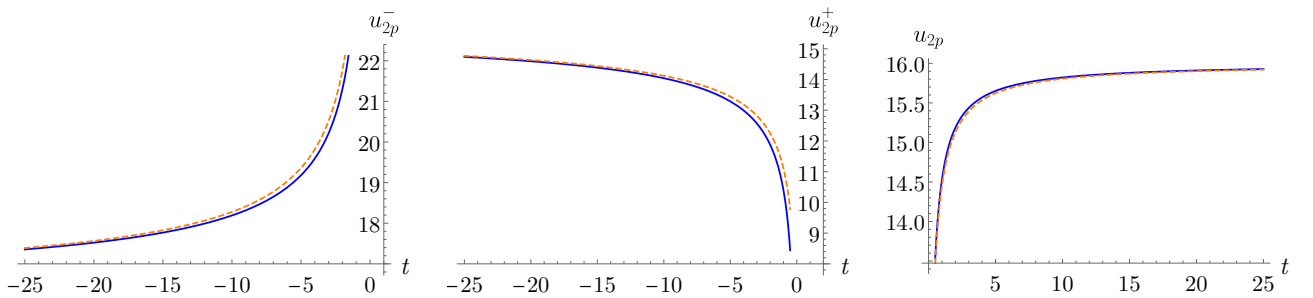


Figure 5: 2-lump peak heights:  $u_{2p}^{\pm}$  vs  $t$  (left two panels),  $u_{2p}$  vs  $t$  (right panel). Exact heights – solid blue line, approximate heights (see (3.6)) – orange dashed line.

To compare with (3.5), we also list below the approximate peak locations  $(r_p, s_p)$  obtained by minimizing  $F_2$

$$(r_p, s_p) = \left( \pm \sqrt{6b|t|} - \frac{1}{2b} \mp \frac{\sqrt{6}}{16b^{5/2}} \frac{1}{|t|^{1/2}} + O\left(\frac{1}{|t|}\right), \quad 0 \right), \quad t \ll 0,$$

$$(r_p, s_p) = \left( -\frac{1}{16b^4} \frac{1}{t} + O\left(\frac{1}{t^2}\right), \quad \pm \sqrt{6bt} + O\left(\frac{1}{t^{3/2}}\right) \right), \quad t \gg 0,$$

as well as the exact values obtained by maximizing  $u_2$

$$(r_p, s_p) = \left( \pm \sqrt{6b|t|} - \frac{1}{2b} \mp \frac{\sqrt{6}}{24b^{5/2}} \frac{1}{|t|^{1/2}} + O\left(\frac{1}{|t|^{3/2}}\right), \quad 0 \right), \quad t \ll 0,$$



$$(r_p, s_p) = \left( -\frac{1}{24b^4} \frac{1}{t} + O\left(\frac{1}{t^2}\right), \quad \pm\sqrt{6bt} \pm \frac{\sqrt{6}}{48b^{5/2}} \frac{1}{t^{1/2}} + O\left(\frac{1}{t^{3/2}}\right) \right), \quad t \gg 0.$$

It is clear that (3.5) gives the leading order peak locations and differ from the exact values by  $O(|t|^{-1/2})$ . Hence, (3.5) can be employed to examine the asymptotic behavior of the 2-lump solution for large  $|t|$ . Substituting  $r = r_p + h, s = s_p + k$  into the expression for  $F_2$  in (3.4), using the first expression from (3.5), and retaining the leading order terms in  $|t|$  for  $t \ll 0$ , yields

$$F_2 = 6b|t| \left[ h^2 + k^2 + \frac{1}{4b^2} + O(|t|^{-1/2}) \right].$$

The leading order expression inside the square brackets of the above equation is precisely the 1-lump polynomial  $F_1(h, k)$  given above (3.3) with  $h = r - r_p, k = s - s_p$ . Then, asymptotically as  $t \rightarrow -\infty$ , the 2-lump solution  $u_2$  can be viewed as a superposition of two 1-lump solutions whose peaks are located at  $(r, s) = (\pm\sqrt{6b|t|}, 0)$ , each with height  $16b^2$ . A similar calculation shows also that  $u_2$  is a superposition of two 1-lumps with peaks at  $(r, s) = (0, \pm\sqrt{6bt})$  and height  $16b^2$ , asymptotically as  $t \rightarrow \infty$  so that the  $L^2$ -norm  $\iint_{\mathbb{R}^2} u_2^2 = 2(16\pi b)$  for all  $t$ .

### Remarks

- (a) If the parameters  $(\gamma_1, \gamma_2) \neq (0, 0)$  then each of the peak locations  $(r_p, s_p)$  shifts by a constant  $(r_0, s_0)$  and the trajectories of the peaks are hyperbolas in the  $rs$ -plane given by  $(r_p - r_0)(s_p - s_0) = \text{constant}$  depending on  $\gamma_1, \gamma_2$ . Otherwise, the asymptotic behavior of the peaks remain essentially the same as above.
- (b) The 2-lump dynamics was discussed in earlier studies [16, 39] as well. But a more detailed discussion of the asymptotic dynamics of the 2-lump solution including the time evolution of the peak heights, are presented in this paper.

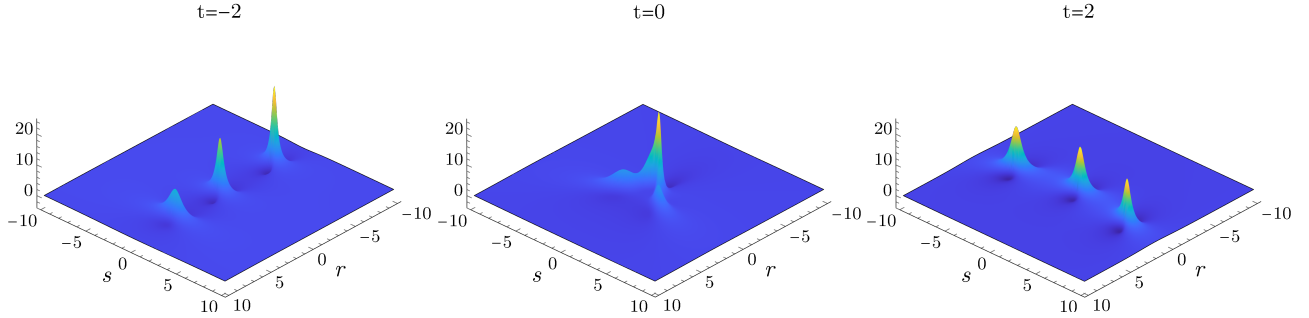


Figure 6: 3-lump solution of the KPI equation:  $a = \gamma_1 = \gamma_2 = \gamma_3 = 0, b = 1$ .

### 3.3 3-lump solution

The 3-lump solutions and its asymptotic dynamics can be analyzed in the same manner as in the 2-lump case. Therefore, we omit most of the details and illustrate the dynamics via Figure 6 which shows the anomalous scattering of a 3-lump solution as the peaks approach along the  $r$ -axis and scatter along the perpendicular  $s$ -axis. The main feature of this solution (and any odd  $n$ -lump) is that the central peak remains on the  $r$ -axis throughout the interaction and moves at a much slower rate than the peaks on its either side.

Equation (2.10) with  $n = 3$  gives the polynomial  $F_3$  whose leading ( $j = 0$ ) term is

$$F_3^{(0)} = \left| \frac{1}{6}r(r^2 - 3s^2) + \frac{1}{4b}(r^2 + s^2) + r(3bt + \frac{1}{4b^2}) + \frac{1}{2}(t + \frac{1}{4b^3}) + i \frac{s}{6}(3r^2 - s^2 + 18bt) \right|^2, \quad (3.7)$$

where we have set the parameters  $\gamma_1 = \gamma_2 = \gamma_3 = 0$ , for simplicity. The approximate location of the peaks are obtained from solving the cubic polynomial equations for  $r$  and  $s$ , resulting from the real and imaginary parts of  $F_3^{(0)} = 0$  in (3.7). The approximate peak locations are given by

$$(r_p, s_p) \approx (\pm\sqrt{18b|t|} - \frac{2}{3b}, 0), \quad (r_p^c, s_p^c) \approx (-\frac{1}{6b} + \frac{29}{972b^4} \frac{1}{|t|}, 0), \quad t \ll 0,$$

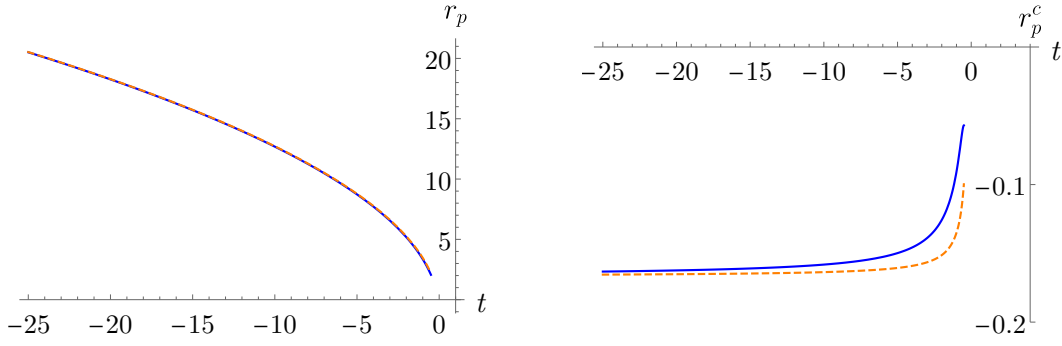


Figure 7: Peak locations ( $t \ll 0$ ). Exact (blue), approximate (orange dashed). Left panel: right peak, reflection across line  $r_p = -\frac{2}{3b}$  gives the left peak location. Right panel: central peak. KP parameters as in Figure 6.

$$(r_p, s_p) \approx \left( \frac{5}{6b} + \frac{83}{1944b^4} \frac{1}{t}, \pm \left( \sqrt{18bt} + \frac{25\sqrt{2}}{144b^{5/2}} \frac{1}{t^{1/2}} \right) \right), \quad (r_p^c, s_p^c) \approx \left( -\frac{1}{6b} - \frac{29}{972b^4} \frac{1}{t}, 0 \right), \quad t \gg 0, \quad (3.8)$$

where  $(r_p, s_p)$  denote the right (or left) peak locations if  $t \ll 0$ , or the top (or bottom) peak locations if  $t \gg 0$ , and  $(r_p^c, s_p^c)$  denotes the central peak locations. The exact and approximate peak locations from (3.8) plotted in Figures 7 and 8 are generally in good agreement for large  $|t|$ . However, since the exact and approximate values differ by  $O(|t|^{-1/2})$  like the 2-lump case, the approximate value of  $r_p(t)$  for  $t \gg 0$ , obtained by minimizing  $F_3$  gives a better approximation  $r_p(t) = \frac{5}{6b} - \frac{451}{6^5} \frac{1}{t}$  than the corresponding formula in (3.8). The difference between the two approximations is in the  $O(t^{-1})$  term.

When  $t \ll 0$ , the three peaks are well separated along the  $r$ -axis with the central peak between  $r = -\frac{1}{6b}$  and  $r = 0$ . Then with increasing time the left and right peaks approach each other and overlap with the central peak near the origin. As time evolves, the 3-lump solution then splits again into three distinct peaks, the central peak remaining on the  $r$ -axis while the other two peaks separate from each other along the  $s$ -axis. All three peak velocities have a small  $r$ -component which is the same for the top and bottom peaks while the central peak travels a bit slower as can be seen from the right panel of Figure 6. Notice that the relative rate of attraction (repulsion) between the left, right (top, bottom) is  $\sqrt{18b}|t|^{-1/2}$  asymptotically as  $|t| \rightarrow \infty$ . The peak trajectories in the  $xy$ -plane can be obtained using (3.1) and (3.8) as in the 2-lump case but are not shown here.

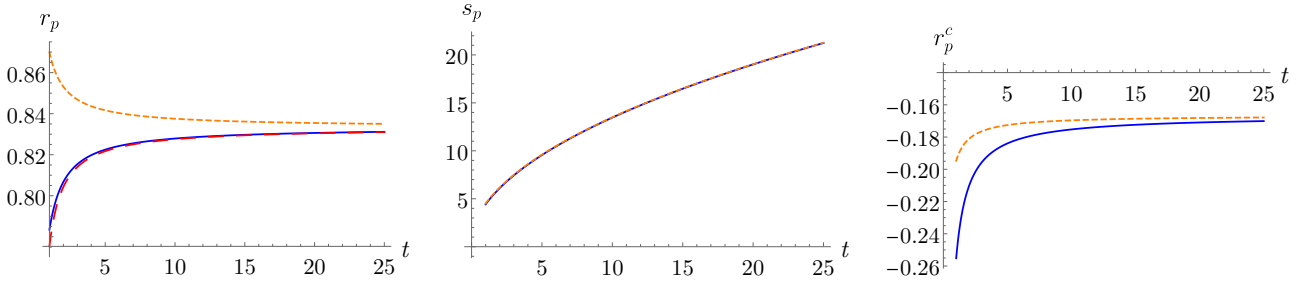


Figure 8: Peak locations ( $t \gg 0$ ). Exact – solid blue, approximate from (3.8) – orange dashed. Left panel:  $r_p(t)$  for top and bottom peaks, the red-dashed curve corresponds to minimum of  $F_3$ . Middle panel:  $s_p(t)$  (top peak)  $= -s_p(t)$  (bottom peak). Right panel: central peak. KP parameters: same as in Figure 6.

The approximate peak heights are obtained by computing  $u_{3p} = u_3(r_p, s_p)$  with  $(r_p, s_p)$  from (3.8) like in the 2-lump case. These are given by

$$\begin{aligned} u_{3p}^{\pm} &\approx 16b^2 \left( 1 \mp \frac{1}{\sqrt{2b^3}} \frac{1}{|t|^{1/2}} + \frac{5}{18b^3} \frac{1}{|t|} \right), & u_{3p}^c &\approx 16b^2 \left( 1 + \frac{7}{36b^3} \frac{1}{|t|} \right), & t &\ll 0, \\ u_{3p}^{\pm} &\approx 16b^2 \left( 1 - \frac{5}{18b^3} \frac{1}{t} \right), & u_{3p}^c &\approx 16b^2 \left( 1 - \frac{7}{36b^3} \frac{1}{t} \right), & t &\gg 0, \end{aligned}$$

where  $u_{3p}^{\pm}, u_{3p}^c$  denote right or left (top or bottom) and the central peak heights, respectively. There are a few features to note from the above formulas which are plotted in Figure 9. First, as  $t \rightarrow -\infty$  each peak height

approach the asymptotic value of  $16b^2$ . Secondly, both the left and the central peak grow as time evolves, whereas the right peak height decreases. Moreover, the left peak grows at a faster rate than the central peak so that for  $t \ll 0$ , the peak heights are *ordered* with the left peak being the highest. After interaction, all the peaks grow at approximately the same rate as each peak height approach 1-lump value of  $16b^2$  as  $t \rightarrow \infty$ .

Finally, we remark that by using local coordinates  $(r, s) = (r_p + h, s_p + k)$  near each peak, the polynomial  $F_3$  reduces to leading order in  $t$ , to a 1-lump polynomial  $F_1(r, s)$ . This implies that the 3-lump solution  $u_3$  is a superposition of three 1-lump solution as  $|t| \rightarrow \infty$ . In fact, it will be shown in Section 4 that the  $n$ -lump solution is a superposition of  $n$  1-lump solutions as  $|t| \rightarrow \infty$ . However, there are no asymptotic shifts in the peak centers before and after collision as in solitonic interactions e.g., the KdV solitons.

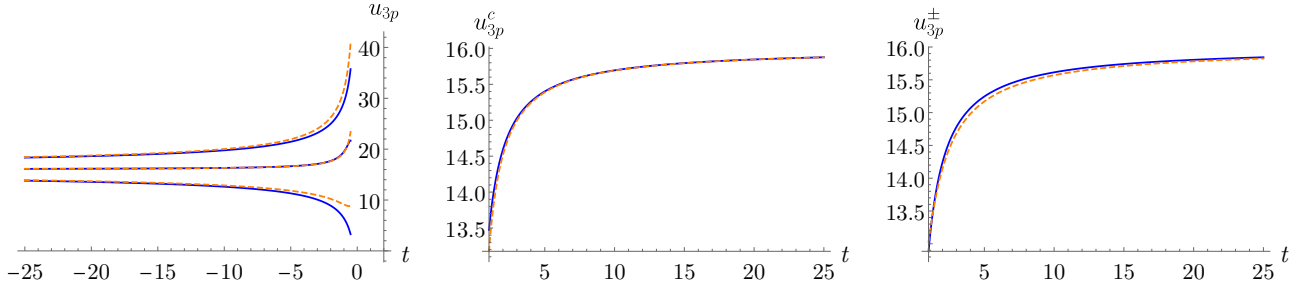


Figure 9: Evolution of 3-lump peak heights. Left panel:  $u_{3p}^-$  (top plot),  $u_{3p}^c$  (middle plot), and  $u_{3p}^+$  (bottom plot) for  $t \ll 0$ . Middle panel:  $u_{3p}^c$ , right panel:  $u_{3p}^\pm$  for  $t \gg 0$ . KP parameters: same as in Figure 6.

## 4 $n$ -lump asymptotics

It is evident from the examples in Section 3 that the  $n$ -lump solution for  $n = 2, 3$  separates into  $n$  distinct peaks whose heights approach the 1-lump peak height asymptotically as  $|t| \rightarrow \infty$ . Moreover, the peak locations scale as  $|t|^{1/2}$  and admit an asymptotic expansion as  $|t| \rightarrow \infty$  in the form of

$$z_j(t) := r_j(t) + is_j(t) \sim |t|^{1/2} (\xi_{j0} + \xi_{j1}\epsilon + \xi_{j2}\epsilon^2 + \dots), \quad \epsilon = |t|^{-1/2},$$

where  $z_j(t)$  is the  $j^{\text{th}}$  peak location,  $j = 1, 2, \dots, n$ . In this section, we will show that the features of the  $n$ -lump solutions discussed in Section 3, also hold for any positive integer  $n$ . The key point of the analysis is the fact that to leading order, the peak locations are given by  $F_n^{(0)}(r, s, t) = 0$  where  $F_n^{(0)}$  is the  $j = 0$  term in the outer sum of (2.10). This fact will be justified in the Appendix.

Utilizing (2.5c) the sum inside  $|\cdot|^2$  of  $F_n^{(0)}$  can be expressed as a *single* generalized Schur polynomial

$$\sum_{l=0}^n \left(\frac{i}{2b}\right)^l p_{n-l} = p_n(\theta_1 + h_1, \theta_2 + h_2, \dots, \theta_n + h_n) := \tilde{p}_n \quad (4.1)$$

by appropriately choosing the  $h_j$ 's such that  $p_j(h_1, \dots, h_j) = (\frac{i}{2b})^j$ . Thus  $p_1(h_1) = h_1 = \frac{i}{2b}$  so that from (3.2),  $\theta_1 + h_1 = i(r + \frac{1}{2b} + is + \gamma_1)$  and all other  $h_j$ 's can be computed successively. Since  $F_n^{(0)} = 0$  implies  $\tilde{p}_n(r, s, t) = 0$ , the approximate peak locations are simply given by the zeros of the generalized Schur polynomial  $\tilde{p}_n$ , to leading order in  $|t|$ . Recall from (3.2), that the  $t$ -dependence in  $\tilde{p}_n$  occurs via  $\theta_2, \theta_3$  which are linear in  $t$ . Then from (2.4),

$$\tilde{p}_n(r, s, t) \sim \sum_{m_1, m_2, m_3 \geq 0} \frac{\theta_1^{m_1} \theta_2^{m_2} \theta_3^{m_3}}{m_1! m_2! m_3!}, \quad \text{with } m_1 + 2m_2 + 3m_3 = n,$$

when  $|t| \gg 0$  since  $\theta_j + h_j$  for  $j > 3$  are constants. In order to find the terms with highest power of  $|t|$  in  $\tilde{p}_n$ , one needs to maximize  $m_2 + m_3$  subject to  $m_1 + 2m_2 + 3m_3 = n$ . It is convenient to consider even and odd  $n$  cases

separately. When  $n = 2m$ , the maximizer is  $(m_1, m_2, m_3) = (0, m, 0)$  so that the term with largest power of  $|t|$  arises from  $\theta_2^m/m!$  which is  $O(|t|^m)$ . When  $n = 2m + 1$ , there are two cases: (i)  $(m_1, m_2, m_3) = (1, m, 0)$  and (ii)  $(m_1, m_2, m_3) = (0, m - 1, 1)$  leading to the terms  $\frac{1}{m!}\theta_1\theta_2^m$  and  $\frac{1}{(m-1)!}\theta_2^{m-1}\theta_3$  respectively, in  $\tilde{p}_n$ . The highest power of  $|t|$  in both those terms are  $|t|^m$ . Then the dominant balance required to solve the equation

$$\tilde{p}_n(r, s, t) = 0$$

asymptotically for  $|t| \gg 0$  arises from the following two cases:

$$(a) \theta_1^{2m} \sim \theta_2^m, \quad n = 2m, \quad \text{and} \quad \theta_1^{2m+1} \sim \theta_1\theta_2^m, \quad n = 2m + 1 \quad (b) \theta_1\theta_2^m \sim \theta_2^{m-1}\theta_3, \quad n = 2m + 1.$$

Case (a) gives the scaling  $\theta_1 \sim \theta_2^{1/2} \sim O(|t|^{1/2})$  as seen earlier for the left/right (top/bottom) peak locations for the 2- and 3-lump solutions, whereas case (b) implies  $\theta_1 \sim O(1)$  as seen for the central peak locations for the 3-lump solution. Collecting all the dominant terms which are  $O(|t|^{n/2})$  from  $\tilde{p}_n$  for case (a), yields

$$\tilde{p}_n(r(t), s(t), t) \sim \sum_{m_1, m_2 \geq 0} \frac{\theta_1^{m_1} \theta_2^{m_2}}{m_1! m_2!} + O(|t|^{(n-1)/2}) \sim i^n \sum_{m_1, m_2 \geq 0} \frac{z^{m_1} (3bt)^{m_2}}{m_1! m_2!} + O(|t|^{(n-1)/2}), \quad (4.2a)$$

with  $m_1 + 2m_2 = n$ . The second expression above is obtained by retaining the dominant terms in  $\theta_1, \theta_2$  from (3.2) and defining  $z(t) = r(t) + is(t)$  which is  $O(|t|^{1/2})$ . Similarly, the dominant terms corresponding to case (b) are given by

$$\tilde{p}_n(r(t), s(t), t) \sim \frac{\tilde{\theta}_1 \tilde{\theta}_2^m}{m!} + \frac{\tilde{\theta}_2^{m-1} \tilde{\theta}_3}{(m-1)!} + O(|t|^{m-1}) \sim i^n \left( \frac{(3bt)^m z}{m!} - \frac{(3bt)^{m-1} t}{(m-1)!} + O(|t|^{m-1}) \right), \quad (4.2b)$$

where  $2m + 1 = n$ ,  $\tilde{\theta}_j = \theta_j + h_j$ ,  $j = 1, 2, 3$  and  $z(t) = (r(t) - r_0) + \frac{1}{2b} + i(s(t) - s_0)$ . Note that since  $\theta_1 \sim O(1)$  in this case, all constant terms are retained leading to a different expression of  $z(t)$  than in (4.2a). The constants  $r_0, s_0$  are determined by the parameters  $\gamma_1, \gamma_2$ , as usual.

#### 4.1 Asymptotic peak locations

First we consider case (b) above where  $n$  is odd and  $z(t) \sim O(1)$ . It follows immediately from (4.2b) that  $\tilde{p}_n = 0$  implies  $z(t) \sim \frac{m}{3b} + O(\frac{1}{|t|})$ . Therefore, when  $n = 2m + 1$ , the location of one of the peaks of the  $n$ -lump solution, to leading order, is given by

$$r(t) = r_0 + \frac{2m-3}{6b} + O(\frac{1}{|t|}), \quad s(t) = s_0, \quad m \geq 0, \quad (4.3)$$

for both  $t \ll 0$  and  $t \gg 0$ . This is the central peak located near the origin of the  $rs$ -plane since the remaining peak locations which scale as  $O(|t|^{1/2})$  are located either along the  $r$ - or  $s$ -axis as will be shown next. Notice that the 1-lump peak location from (3.3) and the 3-lump central peak location given by (3.8) in Section 3 correspond to  $m = 0$  and  $m = 1$  respectively, with  $(r_0, s_0) = (0, 0)$ .

The remaining peak locations are obtained from (4.2a). In order to obtain the leading order contribution, we put  $z = |t|^{1/2}\xi$  in the first term inside the sum of the second expression in (4.2a) to obtain

$$\tilde{p}_n(r(t), s(t), t) \sim |t|^{n/2} h_n(\xi, \eta) + O(|t|^{(n-1)/2}),$$

where  $h_n$  is a two-dimensional elementary Schur polynomial also referred to as the heat polynomial [33] in  $\xi$  and  $\eta = \pm 3b$ , the  $\pm$  sign depends on whether  $t \gg 0$  or  $t \ll 0$ , respectively. Similar to the generalized Schur polynomials introduced in Section 2.1, the heat polynomials have the generating function

$$\exp(\lambda\xi + \lambda^2\eta) = \sum_{n=0}^{\infty} h_n(\xi, \eta) \lambda^n, \quad h_n(\xi, \eta) = \sum_{p, q \geq 0} \frac{\xi^p \eta^q}{p! q!}, \quad p + 2q = n, \quad \eta = \pm 3b \quad (4.4)$$

and have the following useful properties

$$(a) \partial_\xi h_n = h_{n-1}, \quad (b) (n+1)h_{n+1} = \xi h_n + 2\eta h_{n-1}, \quad (c) h_n(-\xi, \eta) = (-1)^n h_n(\xi, \eta) \quad (\text{parity}), \quad (4.5)$$

for  $n \geq 1$ . The first few heat polynomials are given by  $h_0 = 1$ ,  $h_1 = \xi$ ,  $h_2 = \frac{\xi^2}{2} + \eta$ ,  $\dots$ . Thus, by setting  $\tilde{p}_n = 0$  in (4.2a), the leading order peak locations are given by  $z_j(t) = r_j(t) + is_j(t) = |t|^{1/2} \xi_j$  where  $\xi_j$ ,  $j = 1, 2, \dots, n$  are the complex roots of the heat polynomial  $h_n$  regarded as a polynomial in complex variable  $\xi$  only, with a fixed real parameter  $\eta$ . It remains to show that the roots are distinct. This is accomplished by Lemma 1 below whose proof is elementary.

**Lemma 1.** *The heat polynomials  $h_n(\xi, \eta)$  has a root at  $\xi = 0$  when  $n$  is odd. Moreover,  $h_n$  has  $n$  distinct real (in  $\xi$ ), roots if  $\eta < 0$ , and  $n$  distinct, pure imaginary (in  $\xi$ ) roots if  $\eta > 0$ .*

*Proof.* The first part follows from property (c) in (4.5) when  $n$  is odd.

If  $\eta < 0$ , one proceeds by induction. The lemma clearly holds for the base case  $h_1(\xi, \eta) = \xi$ . Assume it holds for  $n \geq 1$ , then it follows from properties (a) and (b) of (4.5) that  $(n+1)h_{n+1} = 2\eta h'_n$  at each root of  $h_n$ , where  $h'_n$  is the derivative with respect to  $\xi$ . Since  $h'_n$  changes sign at consecutive roots of  $h_n$ , so does  $h_{n+1}$ . Therefore,  $h_{n+1}$  has at least  $n-1$  distinct roots, each between two successive roots of  $h_n$ . Since for any  $n$ ,  $h_n \rightarrow \infty$  as  $\xi \rightarrow \infty$  along the real  $\xi$ -axis,  $h'_n > 0$  at the  $n^{\text{th}}$  root of  $h_n$  where consequently,  $h_{n+1} < 0$ . Hence,  $h_{n+1}$  has another root to the right of the  $n^{\text{th}}$  root of  $h_n$ . Thus,  $h_{n+1}$  has at least  $n$  distinct roots. But since  $h_{n+1}$  is a polynomial in  $\xi$  with real coefficients depending on the real parameter  $\eta$ , its roots are either real or complex conjugate pairs. Therefore,  $h_{n+1}$  must have  $n+1$  real, distinct roots.

For  $\eta > 0$ , first put  $\xi = i\hat{\xi}$  and note that  $i^p = i^{n-2q} = i^n(-1)^q$  if  $p+2q = n$ . Then from (4.4) it follows that  $h_n(\xi, \eta) = i^n h_n(\hat{\xi}, -\eta)$ . Thus  $h_n(\hat{\xi}, -\eta)$  has  $n$  distinct, real roots when  $\eta > 0$ . Therefore,  $h_n$  has  $n$  distinct, purely imaginary roots in  $\xi$  including the root  $\xi = 0$  when  $n$  is odd.  $\square$

In summary, Lemma 1 and discussions preceding it demonstrate that to leading order in  $|t|$ , the peaks of a  $n$ -lump solution are separated into  $n$  distinct peaks along the  $r$ -axis located at

$$z_j(t) \sim |t|^{1/2} [(\xi_j, 0) + O(|t|^{-1/2})], \quad t \ll 0, \quad (4.6a)$$

and along the  $s$ -axis at

$$z_j(t) \sim |t|^{1/2} [(0, \xi_j) + O(t^{-1/2})], \quad t \gg 0, \quad (4.6b)$$

for each  $j = 1, 2, \dots, n$ . Moreover, the  $\xi_j$ 's correspond to the real roots of the heat polynomial  $h_n(\xi, \eta)$  defined in (4.4) with  $\eta = -3b$ . When  $n = 2m+1$  is odd, the central peak is located on the  $r$ -axis, given by (4.3), and corresponds to the root  $\xi = 0$  of  $h_n(\xi, \eta)$  (see remark below).

## Remarks

- (a) The heat polynomials  $h_n(\xi, \eta)$  satisfies the heat equation  $h_{\xi\xi} = h_\eta$  in two-dimensions. They are closely related to the Hermite polynomials via  $h_n(\xi, \eta) = \frac{(-\eta)^{n/2}}{n!} H_n(z)$ ,  $z = \xi(-4\eta)^{-1/2}$  [33]. It is well known that the zeros of the Hermite polynomials are real for real  $z$ .
- (b) Although we do not include here, it is possible to obtain the full asymptotic expansion for the roots  $z(t)$  of  $\tilde{p}_n = 0$  by retaining the lower order terms in (4.2a). By setting  $z(t) = |t|^{1/2} \xi$  in (4.2a) and dividing by the leading power  $|t|^{n/2}$ , one finds that  $\tilde{p}_n = 0$  implies that  $h_n(\xi, \eta) + O(\epsilon) = 0$  where  $\epsilon = |t|^{-1/2}$ . Substituting the expansion  $\xi = \xi_0 + \epsilon \xi_1 + \dots$  into this equation one can then calculate the  $\xi_j$ 's. The leading term  $\xi_0$  satisfies  $h_n(\xi_0, \eta) = 0$ , and one can show that the  $O(\epsilon)$  coefficient  $\xi_1$  is real so that  $z(t) = \epsilon^{-1} \xi_0 + \xi_1 + O(\epsilon)$ . This then explains that for odd  $n$ , if  $\xi_0 = 0$  then the central peak location is real for  $|t| \gg 0$  and is given by  $z(t) = \xi_1 + O(\epsilon)$  as shown in (4.3).

## 4.2 Asymptotic peak heights

The approximate peak heights are obtained by calculating  $u_j = u(z_j(t))$  where  $z_j(t) = (r_j(t), s_j(t))$  are the approximate peak locations given by  $F_n^{(0)} = 0$  and whose asymptotic expressions were given in Section 4.1. We decompose the polynomial  $F_n$  in (2.10) as  $F_n = F_n^{(0)} + l$  where  $l$  denotes all other square terms in the outer sum starting from  $j = 1$ . Then the  $n$ -lump solution at  $z_j(t)$  can be expressed as

$$u_n = 2\partial_{xx} \ln(F_n^{(0)} + l) = 2\frac{F_{nxx}^{(0)} + l_{xx}}{l} - 2\left(\frac{F_{nx}^{(0)} + l_x}{l}\right)^2.$$

Writing  $F_n^{(0)} = |A + iB|^2 = A^2 + B^2$ , one obtains  $F_{nx}^{(0)} = 2(AA_x + BB_x) = 0$  and  $F_{nxx}^{(0)} = 2(A_x^2 + B_x^2)$  after using the fact that  $A = B = 0$  at  $z = z_j(t)$ . Furthermore,  $A_x^2 + B_x^2 = |A_x + iB_x|^2 = |\tilde{p}_{n-1}|^2$  which follows from  $\tilde{p}_{nx} = i\partial_{\theta_1}\tilde{p}_n$  and (2.5a). Therefore,

$$u_n(z_j(t)) = 4\frac{|\tilde{p}_{n-1}|^2}{l} + 2\left(\frac{l_{xx}}{l} - \frac{l_x^2}{l^2}\right).$$

We now proceed to estimate  $\tilde{p}_{n-1}$  and  $l$  in the above expression for  $u_n$  at the peak locations. Recall from (4.2a) and (4.2b) that the dominant asymptotic behavior for  $|t| \gg 0$  of the generalized Schur polynomials at the approximate peak locations are given by

$$p_n(z_j(t)) \sim O(|t|^{n/2}), \quad z_j(t) \sim O(|t|^{1/2}), \quad (4.7a)$$

for any positive  $n$ , even or odd, and

$$p_n(z_j(t)) \sim p_{n-1}(z_j(t)) \sim O(|t|^{(n-1)/2}), \quad z_j(t) \sim O(1), \quad (4.7b)$$

when  $n$  is odd. The second estimate follows from the fact that both  $p_n$  and  $p_{n-1}$  has the same highest power of  $|t|$  when  $n$  is odd. This is due to the weighted homogeneity property of the  $p_n$ 's and can be deduced easily from (2.4).

The  $j^{th}$  term in the outer sum of (2.10) starts with  $p_{n-j}$  in the sum inside  $|\cdot|^2$ . Thus it is evident from (4.7a) and (4.7b) that the  $j = 1$  term will dominate in  $l$  when  $|t| \gg 0$ . Using (2.5c) again, the sum inside  $|\cdot|^2$  of the  $j = 1$  term can be expressed as a single generalized Schur polynomial with shifted arguments like in (4.1)

$$\frac{i}{2b} \sum_{m=1}^n m \left(\frac{i}{2b}\right)^{m-1} p_{n-m} = \frac{i}{2b} p_{n-1}(\theta_1 + c_1, \dots, \theta_{n-1} + c_{n-1}) := \frac{i}{2b} \hat{p}_{n-1}, \quad (4.8)$$

where the shifts  $c_j$ 's are determined successively by  $p_j(c_1, \dots, c_j) = (j+1)\left(\frac{i}{2b}\right)^j$  for  $j = 1, \dots, n-1$ . From (4.7a) and (4.7b) one finds that  $\hat{p}_{n-1}(z_j(t)) \sim O(|t|^{(n-1)/2})$ , and that leads to

$$l(z_j(t)) \sim \frac{1}{4b^2} |\hat{p}_{n-1}|^2 + O(|t|^{n-2}), \quad |t| \gg 0. \quad (4.9)$$

Furthermore, the derivatives  $l_x, l_{xx}$  contain polynomials  $p_{n-j}$ ,  $j \geq 2$  and their complex conjugates. Then it follows by using (4.7a) and (4.7b) again that both  $(l_x/l)^2$  and  $l_{xx}/l$  terms are  $O(\frac{1}{|t|})$  at  $z_j(t)$  when  $|t| \gg 0$ . Putting all these estimates together into the above expression  $u_n(z_j(t))$  for the peak height, yields

$$u_n(z_j(t)) \sim 16b^2 \frac{|\tilde{p}_{n-1}|^2}{|\hat{p}_{n-1}|^2} + O\left(\frac{1}{|t|}\right). \quad (4.10)$$

The generalized Schur polynomials  $\tilde{p}_{n-1}$  and  $\hat{p}_{n-1}$  in (4.1) and (4.8) are of the same degree but only with shifted arguments. Hence, one can be expressed in terms of the other by using (2.5c) so that  $\tilde{p}_{n-1} = \hat{p}_{n-1} + O(|t|^{(n-2)/2})$  from (4.7a) or (4.7b). Consequently,  $\tilde{p}_{n-1}/\hat{p}_{n-1} \sim 1 + O(\frac{1}{|t|^{1/2}})$  at each peak location  $z_j(t)$ . Then from (4.10),

it follows that asymptotically as  $|t| \rightarrow \infty$ , each peak height  $u_n(z_j(t)) \sim 16b^2$  for  $j = 1, \dots, n$ , as claimed at the beginning of this section.

An interesting result follows from (4.10) regarding the ordering of the peak heights for  $t \ll 0$ , that was observed for the 3-lump solution in Section 3.3 (see left panel of Figure 9). It was shown in Section 4.1 that  $\tilde{p}_n \sim |t|^{n/2} h_n(\xi, \eta)$  for a positive integer  $n$ . Then,  $\tilde{p}_{n-1}(z(t)) \sim |t|^{(n-1)/2} h_{n-1}(\xi, \eta)$  and  $\hat{p}_{n-1}(z(t)) \sim |t|^{(n-1)/2} h_{n-1}(\xi + \epsilon_1, \eta)$  where the shift  $\epsilon_1$  is obtained as follows. From (4.1) and (4.8) one can see that  $\theta_1$  is shifted by different amounts namely,  $h_1 = \frac{i}{2b}$  and  $c_1 = \frac{i}{b}$  in  $\tilde{p}_n$  and  $\hat{p}_n$ , respectively. This induces an additional shift  $z(t) \rightarrow z(t) + \frac{1}{2b}$  in the argument of  $\hat{p}_{n-1}$ . Hence, after the scaling  $z(t) = |t|^{1/2} \xi$ , one obtains  $\xi \rightarrow \xi + \epsilon_1$  where  $\epsilon_1 = \frac{\epsilon}{2b}$ ,  $\epsilon = |t|^{-1/2}$ . Then for  $t \ll 0$ , (4.10) can be re-expressed as

$$u_n(z_j(t)) \sim 16b^2 \frac{h_{n-1}^2(\xi_j, -3b)}{h_{n-1}^2(\xi_j + \epsilon_1, -3b)},$$

where  $\xi_j$ ,  $j = 1, \dots, n$  are  $n$  real roots of the polynomial  $h_n(\xi, -3b)$ . Expanding  $h_{n-1}(\xi_j + \epsilon_1)$  and using relations (a), (b) from (4.5), and the fact that  $h_n(\xi_j) = 0$ , yields

$$h_{n-1}(\xi_j + \frac{\epsilon}{2b}) = h_{n-1}(\xi_j) + \frac{\epsilon}{2b} h_{n-2}(\xi_j) + O(\epsilon^2) = h_{n-1}(\xi_j) \left( 1 + \frac{\epsilon \xi_j}{12b^2} \right) + O(\epsilon^2).$$

Substituting this into the above expression for  $u_n(z_j(t))$  gives

$$u_n(z_j(t)) \sim \frac{16b^2}{\left(1 + \frac{\xi_j \epsilon}{12b^2}\right)^2} + O(\epsilon^2),$$

which demonstrates that the  $n$ -lump peak heights are in descending order from left to right for  $t \ll 0$ . Note that for the central peak, when  $\xi_j = 0$ , it is necessary to compute the  $O(\epsilon^2)$  contribution to  $u_n(z_j(t))$ .

### 4.3 Asymptotic form of solution and a dynamical system

This subsection is devoted to certain topics arising from the asymptotic analysis developed in Sections 4.1 and 4.2. First we deduce the long time asymptotics of the general  $n$ -lump solution of KPI; then we derive a dynamical system for the zeros  $\xi_j$  of the heat polynomials  $h_n(\xi, \eta)$ .

#### 4.3.1 Asymptotic form of $n$ -lump solution

We begin by deriving the local form of the polynomial  $F_n$  near each peak location  $z_j(t)$   $j = 1, \dots, n$ . As before, we denote  $z := (r, s)$ ,  $z_j(t) = (r_j(t), s_j(t))$ , and put  $z = z_j(t) + (h, k)$  in  $F_n = F_n^{(0)} + l = |\tilde{p}_n|^2 + l$ . Then we expand in  $h, k$  and retain the leading order terms in  $|t|$  in  $F_n$ . Using (3.1), (2.5a) and the fact that  $\tilde{p}_n(z_j(t)) = 0$ , one obtains

$$\tilde{p}_n(z) = (ih - k)\tilde{p}_{n-1}(z_j(t)) + \frac{i}{2b}k\tilde{p}_{n-2}(z_j(t)) + Q(h, k),$$

where  $Q(h, k)$  consists of quadratic and higher powers in  $h, k$  whose coefficients are expressed in terms of  $\tilde{p}_{n-l}$ ,  $l \geq 2$ . Employing (4.7a) and (4.7b) to estimate the dominant behavior of  $p_l(z_j(t))$  in  $F_n^{(0)}$  then yields,

$$|\tilde{p}_n|^2(z) \sim (h^2 + k^2)|\tilde{p}_{n-1}|^2(z_j(t)) + O(|t|^{n-2}).$$

It was shown in Section 4.2 that the dominant term in  $l$  arises from the  $j = 1$  term of (2.10) and its leading order contribution for  $|t| \gg 0$  is

$$l(z) \sim \frac{1}{4b^2}|\hat{p}_{n-1}|^2(z_j(t)) + O(|t|^{n-2}) \sim \frac{1}{4b^2}|\tilde{p}_{n-1}|^2(z_j(t)) + O(|t|^{n-2}).$$

Thus the asymptotic form of  $F_n$  is given by

$$F_n(h, k; z_j(t)) \sim |\tilde{p}_{n-1}|^2(z_j(t)) \left( h^2 + k^2 + \frac{1}{4b^2} + O\left(\frac{1}{|t|}\right) \right). \quad (4.11)$$

Finally, substituting (4.11) for each peak location  $(z_j(t))$ ,  $j = 1, \dots, n$  in (2.9) gives

$$u_n(h, k; z_j(t)) \sim u_1(h, k) + O\left(\frac{1}{|t|}\right).$$

Thus we have shown that asymptotically as  $|t| \rightarrow \infty$ ,  $u_n$  is a superposition of  $n$  distinct 1-lump solutions whose peaks are located at  $z_j(t)$ ,  $j = 1, \dots, n$ . Furthermore, since  $\iint_{\mathbb{R}^2} u_n^2$  is time-invariant it follows immediately that  $\iint_{\mathbb{R}^2} u_n^2 = n \iint_{\mathbb{R}^2} u_1^2 + O\left(\frac{1}{|t|}\right) = n \iint_{\mathbb{R}^2} u_1^2 = n(16\pi b)$ .

### 4.3.2 Dynamical system

The heat polynomial  $h_n(\xi, \eta)$  introduced in Section 4.1 is in fact a rescaled version of the polynomial

$$h_n(z, \tau) = \sum_{m_1, m_2 \geq 0} \frac{z^{m_1} \tau^{m_2}}{m_1! m_2!}, \quad m_1 + 2m_2 = n, \quad \tau = 3bt, \quad (4.12a)$$

which is the dominant term in the second expression of the asymptotic expansion in (4.2a). It is easy to see that

$$h_n(z, \tau) = |t|^{n/2} h_n(\xi, \eta), \quad z = |t|^{1/2} \xi, \quad t = \tau/3b, \quad (4.12b)$$

where  $\eta = \pm 3b$  if  $t > 0$  or  $t < 0$ , respectively. For each positive integer  $n$ ,  $h_n(z, \tau)$  is a polynomial solution of the heat equation  $u_\tau = u_{zz}$  with initial condition  $u(z, 0) = h_n(0) = \frac{z^n}{n!}$  whose solution can be expressed as

$$u(z, \tau) = \frac{1}{n!} \exp(\tau \partial_z^2) (z^n) = \frac{1}{n!} \sum_{j=0}^{\infty} \frac{\tau^j}{j!} \partial_z^{2j} (z^n) = h_n(z, \tau).$$

The goal here is to investigate the dynamics of the zeros  $z_k(\tau)$  of  $h_n(z, \tau) = 0$  with respect to the evolution variable  $\tau$ . This is accomplished by differentiating implicitly the equation  $h_n(z_k(\tau), \tau) = 0$ , which yields

$$h_{nz} z'_k(\tau) + h_{n\tau} = h_{nz} z'_k(\tau) + h_{nzz} = 0,$$

after using the heat equation. Now from Lemma 1 and (4.12b) it is clear that  $h_n(z, \tau) = 0$  has  $n$  distinct roots. Hence, it can be expressed as  $h_n(z, \tau) = \frac{1}{n!} (z - z_1(\tau))(z - z_2(\tau)) \cdots (z - z_n(\tau))$  so that the logarithmic derivative

$$h_{nz}/h_n = \sum_{j=1}^n \frac{1}{z - z_j(\tau)}.$$

Moving the  $k^{\text{th}}$  term from the above sum to the left and letting  $z \rightarrow z_k(\tau)$ , one recovers after using L'hospital's rule, a system of ordinary differential equations for the zeros  $z_k(\tau)$ ,  $k = 1, \dots, n$ , namely

$$z'_k(\tau) = - \lim_{z \rightarrow z_k} \frac{h_{nzz}}{h_{nz}} = \sum_{j \neq k} \frac{2}{z_j - z_k}, \quad z_k(0) = 0. \quad (4.13)$$

The dynamical system (4.13) is one of the simplest examples describing the motion of zeros of the solution to a partial differential equation. This system was studied in different contexts such as moving poles of the complex Burger's equation [11, 9], vortex dynamics [7], and more recently in proving certain conjecture related to the Riemann hypothesis [12, 32]. Equation (4.13) can be expressed as a gradient flow of a logarithmic potential

$$z'_k(\tau) = - \frac{\partial V}{\partial z_k}, \quad V = \sum_{\substack{i,j \\ i \neq j}} \log |z_i - z_j|,$$

whose evolution can be computed as follows

$$V'(\tau) = \sum_{k=1}^n z'_k(\tau) \frac{\partial V}{\partial z_k} = - \sum_{k=1}^n \left( \frac{\partial V}{\partial z_k} \right)^2 = - \sum_{k=1}^n \sum_{\substack{i,j \\ i \neq k, j \neq k}} \frac{4}{(z_i - z_k)(z_j - z_k)} = - \sum_{\substack{i,j \\ i \neq j}} \frac{4}{(z_i - z_j)^2},$$



where the cross-terms vanish in the last inequality. Consequently, the acceleration  $z_k''(\tau)$  satisfies

$$z_k''(\tau) = -\frac{\partial V'(\tau)}{\partial z_k} = \sum_{i \neq k} \frac{16}{(z_i - z_k)^3},$$

which is the well-known Calogero-Moser system [8]. Thus, (4.13) implies that the  $z_k$ 's satisfy the Calogero-Moser system although the converse is not necessarily true.

A complete description of the zeros of the polynomial  $h_n(z, \tau)$  is of course readily available from the transformation given in (4.12b) in terms of the polynomials  $h_n(\xi, \eta)$  and particularly, Lemma 1 of Section 4.1. For  $\tau < 0$ , the zeros  $z_k(\tau) = r_k(\tau) + is_k(\tau) = (\frac{|\tau|}{3b})^{1/2} \xi_k$  are real, distinct, and symmetrically located about the origin along the  $r$ -axis, they all coalesce at  $\tau = 0$  and emerge along the  $s$ -axis as purely imaginary and complex conjugate roots for  $\tau > 0$ . Nonetheless, one gains further insights into their dynamics from analyzing the system (4.13). Fix a  $\tau_0 < 0$  and consider the interval  $I = [z_k(\tau_0), z_{k+1}(\tau_0)]$ . Clearly the first derivative  $h_{nz}$  has opposite signs at the zeros  $z_k(\tau_0)$ , and  $z_{k+1}(\tau_0)$ . Now suppose that the derivative  $h_{nz}$  is positive at  $z_k(\tau_0)$  and negative at  $z_{k+1}(\tau_0)$  so that the concavity  $h_{nzz} < 0$  on  $I$ , then from (4.13) it follows that  $z_k'(\tau_0) > 0$  whereas  $z_{k+1}'(\tau_0) < 0$ , which means that the zeros behave like point particles attracting each other for  $\tau < 0$ . The conclusion remains the same if the sign of  $h_{nz}$  is reversed at the end points of the interval  $I$ . In this situation, the logarithmic potential  $V(\tau)$  is a monotonically decreasing function of  $\tau$  since  $V'(\tau) < 0$ , and reaches a singularity ( $V \rightarrow -\infty$ ) when all the zeros collide at  $\tau = 0$ . An opposite scenario is observed for  $\tau > 0$  by replacing  $z_j(\tau) = i\zeta_j(\tau)$  in (4.13), and  $\zeta_j(\tau)$  is now real. The zeros now repel from each other and  $V(\tau)$  increases monotonically in  $\tau$  as the zeros move further apart from each other. From the viewpoint of point particle dynamics the force of attraction (repulsion) is given by the Calogero Moser system above depending on if the  $z_k$ 's are real (pure imaginary) for  $\tau < 0$  ( $\tau > 0$ ).

In conclusion, we have demonstrated that the  $n$ -lump solution of the KPI equation splits into  $n$  distinct peaks for  $|t| \gg 0$  whose locations evolve as  $n$  interacting point particles as given by (4.13). However, the dynamics only describe the leading order peak locations for large  $|t|$  and can not be used to infer the evolution when  $|t| \sim O(1)$  or smaller.

## Remarks

- (a) Substituting  $z_k(\tau) = (\frac{|\tau|}{3b})^{1/2} \xi_k$  in (4.13) gives the following relations among the roots  $\xi_k$  of  $h_n(\xi, \eta)$

$$x_k = \mp \sum_{j \neq k} \frac{1}{x_j - x_k}, \quad \xi_k = 2\sqrt{3b} x_k, \quad 1 \leq k \leq n,$$

where the  $\mp$  sign depends respectively, on whether the roots are real or pure imaginary. These are called the Stieltjes relations [37, 38] for the zeros of the Hermite polynomials. The Stieltjes relations can be used to determine the roots  $x_k$  exactly.

- (b) The dynamical system (4.13) was also obtained in [25, 30] by considering zeros of wronskian  $\tau$ -functions of KPI. This wronskian can in fact be identified with the generalized Schur polynomial  $\tilde{p}_n$  in (4.1). In this paper, it was explicitly shown that the zeros of  $\tilde{p}_n$  are indeed *distinct* for  $|t| \gg 0$ , and dynamical system (4.13) was used to explain the anomalous nature of the  $n$ -lump interaction.

## 5 $n$ -lump eigenfunction

The KPI equation admits a Lax pair which is the following linear system of equations

$$i\psi_y = \psi_{xx} + u\psi, \quad \psi_t = -\psi_{xxx} - \frac{3}{2}u\psi_x - \frac{3}{4}(u_x + iw)\psi, \quad w_x = u_y, \quad (5.1)$$

where the common solution  $\psi(x, y, t)$  is usually called the eigenfunction and  $u(x, y, t)$  is the KPI solution. It follows from the integrability condition  $\psi_{ty} = \psi_{yt}$  of (5.1) that  $u(x, y, t)$  satisfies the KPI equation (1.1). It is

significant to note that the first equation in (5.1) is the well-known non-stationary Schrödinger equation (NSE) with  $u(x, y, t)$  regarded as the potential function parametrized by  $t$ . Thus, any solution of KPI equation at a fixed  $t$  is a potential function and in particular, the  $n$ -lump solution  $u_n(x, y, t)$  belongs to the class of rational potentials for the NSE.

## 5.1 Binary Darboux transformation

The aim of this section is to derive an explicit form for the eigenfunction  $\psi$  of (5.1) associated with the  $n$ -lump potential  $u_n$  by employing binary Darboux transformation [26]. Such eigenfunctions were found via the IST method [3, 39] and the  $\bar{\partial}$ -dressing method [14] in earlier studies which outlined an explicit scheme to construct  $\psi$  and  $u_n$ , and which works well for small  $n$  values. However, the scheme becomes unwieldy to obtain general expressions for  $\psi$  for arbitrary  $n$  – a task that is accomplished by the algebraic method presented here.

Let us first start with solutions of (5.1) when  $u = 0$ . In this case, (5.1) coincides with (2.7). Then it is possible to verify the following lemma by direct calculation.

**Lemma 2.** *Suppose  $\psi_0$  is any solution of (2.7), and  $\phi_n(k_0)$  defined by (2.1) is another particular solution of (2.7) with a fixed complex parameter  $k_0 = a + ib$ . Then*

$$\hat{\psi} = -\frac{M(\psi_0, \bar{\phi}_n)}{\bar{\phi}_n}, \quad M(\psi_0, \bar{\phi}_n) = \int_x^\infty \psi_0 \bar{\phi}_n dx$$

is a solution of (5.1) with  $u = \hat{u} := 2 \ln(\bar{\phi}_n)_{xx}$ .

Recall that  $\bar{\phi}_n$  is the complex conjugate of  $\phi_n$ . The transformation  $(\psi_0, u = 0) \rightarrow (\hat{\psi}, \hat{u})$  is called an adjoint Darboux transformation. Next we introduce an ordinary Darboux transformation.

**Lemma 3.** *Suppose  $(\hat{\psi}, \hat{u})$  satisfies (5.1) as in Lemma 2 and  $\hat{\psi}_n = -M(\phi_n, \bar{\phi}_n)/\bar{\phi}_n$  is a particular solution (5.1) with  $u = \hat{u}$ . Then  $\psi_n = \hat{\psi}_x - \hat{\psi}(\ln \hat{\psi}_n)_x$  is a solution of (5.1) with  $u = \hat{u} + 2 \ln(\hat{\psi}_n)_{xx} = u_n$  where  $u_n$  is the  $n$ -lump solution.*

By replacing  $\psi_0$  by  $\phi_n$  in the expression for  $\hat{\psi}$  of Lemma 2, it should be clear that  $\hat{\psi}_n$  solves (5.1) with  $u = \hat{u}$  as claimed in Lemma 3. It is easy to verify from the definitions of  $\hat{u}, \hat{\psi}_n$ , (2.8) and (2.9) in Section 2.2 that  $\hat{u} + 2 \ln(\hat{\psi}_n)_{xx} = 2 \ln(\bar{\phi}_n)_{xx} + 2 \ln(\hat{\psi}_n)_{xx} = 2 \partial_x^2 \ln M(\phi_n, \bar{\phi}_n) = u_n$ . Thus  $(\hat{\psi}, \hat{u}) \rightarrow (\psi_n, u_n)$  is the ordinary Darboux transformation. The composition of the adjoint and ordinary Darboux transformations gives

$$(\psi_0, u = 0) \xrightarrow{\phi_n, \bar{\phi}_n} (\psi_n, u_n)$$

which is called the binary Darboux transformation that is triggered by the solutions  $\phi_n, \bar{\phi}_n$  of (2.7) or (5.1) with  $u = 0$ . To further clarify this transformation, note that from the definitions of  $\hat{\psi}, \hat{\psi}_n$  in Lemmas 2 and 3, one obtains

$$\psi_n = \hat{\psi} \partial_x \ln(\hat{\psi}/\hat{\psi}_n) = -\frac{M(\psi_0, \bar{\phi}_n)}{\bar{\phi}_n} \partial_x \ln \left( \frac{M(\psi_0, \bar{\phi}_n)}{M(\phi_n, \bar{\phi}_n)} \right).$$

Then after using the fact that  $M(f, g)_x = -fg$  in the above expression, yields the following expression for the  $n$ -lump eigenfunction and the solution

$$\psi_n = \psi_0 - \frac{M(\psi_0, \bar{\phi}_n)}{M(\phi_n, \bar{\phi}_n)} \phi_n, \quad u_n = 2 \partial_x^2 \ln M(\phi_n, \bar{\phi}_n). \quad (5.2)$$

### Remarks

- (a) The binary Darboux transformation is a powerful tool to algebraically generate solutions to many integrable systems [26]. In particular, this method has been used to investigate a broader class of rational solutions of KPI [4].

- (b) It is possible to generate KP I lump solutions by only using the ordinary Darboux transformation prescribed in Lemma 3. This will lead to a wronskian form of the  $\tau$ -function. However, the resulting solutions are in general, singular in  $\mathbb{R}^2$  for any  $t$ .

Our next goal is to highlight certain interesting features of the eigenfunction  $\psi_n$  and their role to characterize the  $n$ -lump NSE potential.

## 5.2 Properties of the eigenfunction

The function  $\psi_0$  that was left arbitrary in (5.2) is now chosen to be  $\psi_0 = A(k) \exp i\theta$  where  $\theta = kx + k^2y + k^3t + \theta_0(k)$ ,  $k \in \mathbb{C}$  an arbitrary complex parameter, and  $A(k)$  to be determined a little later. Inserting this  $\psi_0$  into (5.2) and using  $\phi_n(k_0) = p_n(k_0) \exp i\theta(k_0)$ ,  $k_0 = a + ib$  together with its complex conjugate  $\bar{\phi}_n(k_0)$ , one first computes

$$M(\psi_0, \bar{\phi}_n) = A(k) \sum_{j=0}^n \frac{i\bar{p}_{n-j}(k_0)}{(k - \bar{k}_0)^{j+1}} e^{i(\theta(k) - \bar{\theta}(k_0))}, \quad M(\phi_n, \bar{\phi}_n) = \frac{F_n}{2b} e^{i(\theta(k_0) - \bar{\theta}(k_0))}.$$

by using integration by parts and (2.8),(2.9). Substituting the above expressions back into (5.2) results in the following expression for the eigenfunction

$$\psi_n = \mu(k) e^{i\theta(k)}, \quad \mu(x, y, t, k) = 1 + \frac{(k_0 - \bar{k}_0)}{(k - k_0)} \left[ \frac{(F_n - p_n \bar{p}_n)}{F_n} - \frac{p_n}{F_n} \sum_{j=1}^n \frac{\bar{p}_{n-j}}{(k - \bar{k}_0)^j} \right], \quad (5.3)$$

where  $A(k) = (k - \bar{k}_0)/(k - k_0)$  is chosen to ensure the normalization  $\mu(k) \rightarrow 1$  as  $k \rightarrow \infty$ . It is clear from (5.3) that the reduced eigenfunction  $\mu(k)$  is meromorphic in the complex  $k$ -plane with a simple pole at  $k = k_0$  and a pole of order  $n$  at  $k = \bar{k}_0$ . In fact, by partial fraction decomposition, one can explicitly write

$$\mu = 1 + \frac{\mu_1}{k - k_0} + \sum_{j=1}^n \frac{\mu_{\bar{j}}}{(k - \bar{k}_0)^j},$$

$$\mu_1 = (k_0 - \bar{k}_0) \frac{F_n - p_n \bar{p}_n}{F_n} - \frac{p_n}{F_n} \sum_{l=1}^n \frac{\bar{p}_{n-l}}{(k_0 - \bar{k}_0)^{l-1}}, \quad \mu_{\bar{j}} = \frac{p_n}{F_n} \sum_{l=j}^n \frac{\bar{p}_{n-l}}{(k_0 - \bar{k}_0)^{l-j}}, \quad j = 1, \dots, n. \quad (5.4)$$

It is evident from (5.4) that  $\mu(x, y, t, k)$  is a rational function in  $x, y, t$ . Moreover, for fixed  $t$ , one can deduce from (5.4), (2.10) and (2.4) that  $\mu_1 \sim O(\frac{1}{\theta_1}) \sim O(\frac{1}{R})$ ,  $\mu_{\bar{j}} \sim O(\frac{1}{\theta_1^j}) \sim O(\frac{1}{R^j})$  so that  $\mu \rightarrow 1$  as  $R = \sqrt{x^2 + y^2} \rightarrow \infty$ .

It follows from (5.1) and (5.3) that  $\mu(k)$  satisfies the reduced NSE

$$i\mu_y = \mu_{xx} + 2ik\mu_x + u_n\mu, \quad (5.5)$$

as well as a time evolution equation which is not necessary to include here. Letting  $k \rightarrow \infty$ , one obtains from (5.4) and (5.5) the following relation for the  $n$ -lump solution in terms of the residues at the poles of  $\mu(k)$

$$u_n = -2i(\mu_1 + \mu_{\bar{1}})_x,$$

which provides the NSE potential in terms of the eigenfunction. That is usually the case in the IST method where one solves first for  $\mu(k)$  and then obtains  $u_n$  from it. However, in our case it is possible to verify the above relation from the explicit expressions for  $\mu(k)$  and  $u_n$  that are already available. Since  $\mu_1 + \mu_{\bar{1}} = \frac{2ib}{F_n}(F_n - p_n \bar{p}_n)$  from (5.4) and  $u_n = 2(\ln F_n)_{xx}$ , it suffices to verify that  $F_{nx} = 2b(F_n - p_n \bar{p}_n)$ . The latter follows immediately from the expression of  $F_n$  in (2.9) and noting that  $\partial_x^{2n+1}|p_n|^2 = 0$ .

Near the pole  $k = k_0$ , the reduced eigenfunction in (5.3) can be separated into a singular and regular part  $\mu(k) = \nu(k) + \mu_1/(k - k_0)$  where  $\nu(k)$  is analytic near  $k = k_0$  and  $\nu(k) \rightarrow 1$  as  $k \rightarrow \infty$ . Inserting this decomposition in (5.5), the coefficient of  $(k - k_0)^{-1}$  yields

$$L(k_0)\mu_1 = 0, \quad L(k) = i\partial_y - \partial_{xx} - 2ik\partial_x - u_n,$$

which implies that  $\mu_1(k_0)$  is the eigenfunction of the linear operator  $L(k)$  with eigenvalue  $k = k_0$ . Integrating the equation  $L(k_0)\mu_1 = 0$  over  $\mathbb{R}^2$  for fixed  $t$  and using Green's theorem, one obtains

$$\iint_{\mathbb{R}^2} u_n \mu_1 = \oint_{\Gamma_\infty} -i\mu_1(dx + 2k_0 dy) - \mu_{1x} dy = - \oint_{\Gamma_\infty} \mu_1 d\theta_1,$$

where  $\Gamma_\infty$  is a positively oriented contour at the boundary of  $\mathbb{R}^2$  (i.e.,  $R \rightarrow \infty$ ) surrounding the origin once. The last equality above follows from (2.2) and the fact that  $\mu_{1x} \sim O(\frac{1}{R^2})$ . From (2.10) and (5.4), one obtains as  $R \rightarrow \infty$  that  $\mu_1 = -p_{n-1}/p_n + O(\frac{1}{R^2}) = -\partial_{\theta_1} \log p_n + O(\frac{1}{R^2})$  and from (2.4),  $p_n \sim \theta_1^n/n!$ . Thus,

$$\frac{1}{2\pi i} \iint_{\mathbb{R}^2} u_n \mu_1 = \frac{1}{2\pi i} \oint_{\Gamma_\infty} n \frac{d\theta_1}{\theta_1} = n.$$

The above expression gives the winding number of the generalized Schur polynomial  $p_n$  in the complex  $\theta_1$ -plane, and defines a topological charge [3], which provides another characterization of the  $n$ -lump NSE potential  $u_n$ . In the IST theory the charge is a constraint on the NSE potential required to solve for  $\mu(k)$  in (5.3) in a consistent manner. In a similar way, writing  $\mu(k) = \tilde{\nu}(k) + \mu_{\bar{1}}/(k - \bar{k}_0) + \dots + \mu_{\bar{n}}/(k - \bar{k}_0)^n$ , where  $\tilde{\nu}(k)$  is analytic near  $k = \bar{k}_0$ , the following chain of equations

$$L(\bar{k}_0)\mu_{\bar{j}} = 2i\partial_x \mu_{\bar{j}+1}, \quad j = 1, 2, \dots, n-1, \quad L(\bar{k}_0)\mu_{\bar{n}} = 0$$

are obtained from the coefficients of  $(k - \bar{k}_0)^j$  in (5.5). In this case the linear operator  $L(k)$  has the eigenfunction  $\mu_{\bar{n}}(\bar{k}_0)$  with eigenvalue  $k = \bar{k}_0$ . It is possible to obtain a similar topological relation as above if one integrates the quantity  $u_n \mu_{\bar{1}}$  over  $\mathbb{R}^2$ . Integrating the equation  $L(\bar{k}_0)\mu_{\bar{1}} = 2i\mu_{\bar{2}x}$  arising from the coefficient of  $(k - \bar{k}_0)^{-1}$  and applying Green's theorem yields,

$$\iint_{\mathbb{R}^2} u_n \mu_{\bar{1}} = \oint_{\Gamma_\infty} \mu_{\bar{1}} d\bar{\theta}_1 = n \oint_{\Gamma_\infty} \frac{d\bar{\theta}_1}{\bar{\theta}_1} = -2n\pi i,$$

after using the fact that from (5.4)  $\mu_{\bar{1}x} \sim O(\frac{1}{R^2})$ ,  $\mu_{\bar{2}} \sim O(\frac{1}{R^2})$  as  $R \rightarrow \infty$  (so they do not contribute to the line integral), and  $\mu_{\bar{1}} = \bar{p}_{n-1}/\bar{p}_n + O(\frac{1}{R^2}) = n/\theta_{\bar{1}} + O(\frac{1}{R^2})$ . Combining the two results above, one can give a unified definition of the topological charge as [39]

$$Q(k_\alpha) = \frac{\text{sgn}(\text{Im}(k_\alpha))}{2\pi i} \iint_{\mathbb{R}^2} u_n \text{Res}_{k_\alpha} \mu(k) = n, \quad k_\alpha \in \{k_0, \bar{k}_0\}. \quad (5.6)$$

In fact  $Q(k_0) = Q(\bar{k}_0)$  can also be shown by integrating  $u_n(\mu_1 + \mu_{\bar{1}})$  over  $\mathbb{R}^2$  and using the residue relation  $u_n = -2i(\mu_1 + \mu_{\bar{1}})_x$ . For the sake of completeness we mention that using (5.4) and Green's theorem, it can also be shown that

$$\iint_{\mathbb{R}^2} u_n \mu_{\bar{j}} = 0, \quad 2 \leq j \leq n,$$

since  $\mu_{\bar{j}} \sim O(\frac{1}{R^j})$  as  $R \rightarrow \infty$ . Recall that  $u_n \notin L^1(\mathbb{R}^2)$  since it decays as  $\frac{1}{R^2}$ . The slow decay is the underlying fact why the charge appears.

## Remarks

- (a) Our discussion in Section 5.2 follows closely the spectral theory of KPI rational solution developed in [3, 39] although our approach is algebraic. The explicit expression for  $\mu(k)$  in (5.4) was not presented earlier since the resulting computation via IST becomes rather unwieldy.
- (b) The IST approach in [3, 39] assumes that the kernel of the operator  $L(k_0)$  is one-dimensional. That is known *not* to be true for more general multi-lump solutions of KPI although it has been conjectured [5] that  $\dim(\ker(L(k_0))) = Q + 2 - (m + \bar{m})$  where  $Q$  is the charge and  $m, \bar{m}$  are the order of the poles of  $\mu(k)$  at  $k_0$  and  $\bar{k}_0$ , respectively. It should be interesting to derive the above relation for  $\dim(\ker(L(k_0)))$  via the direct, algebraic approach where  $\mu(k)$  is explicitly constructed by the binary Darboux transformation.

## 6 Concluding remarks

The rational multi-lump solutions of KPI equation had been found earlier but their internal dynamics have not been studied in great details because the underlying formulas are complicated. For this reason, we have considered a special class of solutions that are relatively easier to analyze as well as retain the flavor of anomalous interactions exhibited by such types of rational solutions. We have comprehensively studied the behavior and properties of this class of solutions in this paper. In the future, we plan to investigate the general type of multi-lump solutions of KPI, characterize them and develop a suitable classification scheme. We would also like to relate our work to the IST scheme in the hope of addressing certain open issues.

## 7 Acknowledgments

SC thanks Prof. Mark Ablowitz (CU Boulder) for useful discussions. Early part of this work was partially supported by NSF grant No. DMS-1410862.

## Appendix

### A Approximate vs exact peak locations

Throughout Sections 3 and 4, the approximation  $F_n^{(0)}(r, s, t) = 0$  equivalently,  $\tilde{p}_n(r, s, t) = 0$  was used to obtain the locations of the lump peaks instead of their exact values that are obtained from maximizing  $u_n(r, s, t)$ . As mentioned in Section 3.2, this approximation is based the assumption that the maxima of  $u_n$  are close to the minima of  $F_n$  which again, are close to the zeros of the highest degree polynomial  $F_n^{(0)}$  in the expression (2.10) for  $F_n$ . In fact, the exact and approximate peak locations were shown in Section 3.2 to be off by  $O(|t|^{-1/2})$  for  $|t| \gg 0$  in the case of 2-lump solutions. Here we are going to provide a justification that this approximation is also valid for the  $n$ -lump solution by utilizing the asymptotics developed in Sections 4.2 and 4.3. In the following we will denote the exact peak location by  $z_p := (r_p, s_p)$ , the approximate peak location via minimizing  $F_n$  by  $z_p^{min} = (r_p^{min}, s_p^{min})$ , and the approximate peak location from  $F_n^{(0)} = 0$  by  $z_p^{(0)} = (r_p^{(0)}, s_p^{(0)})$ . Then it will be shown specifically that

$$z_p \sim z_p^{min} + O(|t|^{-1/2}), \quad z_p^{min} \sim z_p^{(0)} + O(|t|^{-1/2}), \quad |t| \gg 0. \quad (\text{A.1})$$

We will give the details of the second asymptotic calculation below and then will briefly outline the first one.

Differentiating  $F_n = F_n^{(0)} + l = A^2 + B^2 + l$  with respect to  $r$  and  $s$  one readily obtains expressions for  $F_{nr} := g$ ,  $F_{ns} := h$  and their derivatives  $g_r$ ,  $h_s$ ,  $g_s = h_r$ . Setting  $A = B = 0$  into these expressions, yields the following at  $z = z_p^{(0)}$

$$\begin{aligned} g &= l_r, & h &= l_s, & g_r &= 2(A_r^2 + B_r^2) + l_{rr}, \\ h_s &= 2(A_s^2 + B_s^2) + l_{ss}, & g_s &= h_r = 2(A_r A_s + B_r B_s) + l_{rs}. \end{aligned}$$

If we linearize  $g$  and  $h$  near  $z = z_p^{(0)}$  and evaluate at  $z = z_p^{min}$  where  $g = h = 0$ , we obtain the following approximate equations

$$\begin{aligned} 0 &= g(z_p^{min}) \approx g(z_p^{(0)}) + \delta r g_r(z_p^{(0)}) + \delta s g_s(z_p^{(0)}) \\ 0 &= h(z_p^{min}) \approx h(z_p^{(0)}) + \delta r h_r(z_p^{(0)}) + \delta s h_s(z_p^{(0)}), \end{aligned} \quad (\text{A.2})$$

which can be regarded as a linear system  $M\delta u = v$  for  $\delta u = (\delta r, \delta s)^T$ ,  $v = -(l_r, l_s)(z_p^{(0)})$ . We next proceed to obtain asymptotic expressions for the entries of the coefficient matrix  $M$  which is real symmetric. It is convenient first to express these entries in terms of generalized Schur polynomials. It is known from (4.9) that  $l(z_p^{(0)}) \sim$

$|\hat{p}_{n-1}|^2 \sim O(|t|^{n-1})$  for  $|t| \gg 0$ . Consequently,  $l_r, l_s \sim O(|t|^{n-3/2})$  and  $l_{rr}, l_{rs}, l_{ss} \sim O(|t|^{n-2})$  at  $z = z_p^{(0)}$ . (Recall that  $z_p^{(0)}$  represents any of the approximate peak locations that were denoted by  $z_j(t)$ ,  $j = 1, \dots, n$  in Sections 4.1 and 4.2). Since  $A + iB = \tilde{p}_n$ , one can express the quantity  $A_r^2 + B_r^2 = |\partial_r(A + iB)|^2 = |\tilde{p}_{n-1}|^2$ , and similarly,  $A_s^2 + B_s^2 = |\partial_s(A + iB)|^2 = |\tilde{p}_{n-1} - \frac{i}{2b}\tilde{p}_{n-2}|^2$  where (3.2) and (2.5a) were used to compute the derivatives. Moreover,  $(A_r + iB_r)(A_s - iB_s) = (A_r A_s + B_r B_s) - i(A_r B_s - A_s B_r) = -i|\tilde{p}_{n-1}|^2 + \frac{1}{2b}\tilde{p}_{n-1}\bar{\tilde{p}}_{n-2}$  where the overbar indicates complex conjugation. Equating the real and imaginary part of the previous expression give  $A_r A_s + B_r B_s = \frac{1}{2b} \operatorname{Re}(\tilde{p}_{n-1}\bar{\tilde{p}}_{n-2})$  and  $A_r B_s - A_s B_r = |\tilde{p}_{n-1}|^2 - \frac{1}{2b} \operatorname{Im}(\tilde{p}_{n-1}\bar{\tilde{p}}_{n-2})$ . Finally, using (4.7a) and (4.7b), the leading order behavior of the entries of the matrix  $M$  for  $|t| \gg 0$  are given as follows

$$\begin{aligned} g_r &\sim 2(A_r^2 + B_r^2) = 2|\tilde{p}_{n-1}|^2 \sim O(|t|^{n-1}), \\ h_s &\sim 2(A_s^2 + B_s^2) = 2|\tilde{p}_{n-1} - \frac{i}{2b}\tilde{p}_{n-2}|^2 \sim 2|\tilde{p}_{n-1}|^2 \sim O(|t|^{n-1}) \\ g_s = h_r &\sim 2(A_r A_s + B_r B_s) = \frac{1}{2b} \operatorname{Re}(\tilde{p}_{n-1}\bar{\tilde{p}}_{n-2}) \sim O(|t|^{n-3/2}), \end{aligned} \quad (\text{A.3})$$

at  $z = z_p^{(0)}$ . It follows from (A.3) that the off diagonal entries of  $M$  in (A.2) are of lower order in  $|t|$  than the diagonal entries. The determinant of  $M$  to leading order in  $|t|$  is given by

$$\det M = g_r h_s - g_s h_r \sim 4(A_r B_s - A_s B_r)^2 = 4(|\tilde{p}_{n-1}|^2 - \frac{1}{2b} \operatorname{Im}(\tilde{p}_{n-1}\bar{\tilde{p}}_{n-2}))^2 \sim 4|\tilde{p}_{n-1}|^4 \sim O(|t|^{2(n-1)}),$$

which shows that  $\det M > 0$ , hence  $M$  is invertible. Then from the solution  $\delta u = (\delta r, \delta s)^T = M^{-1}v$  of the linear system (A.2) one can estimate  $\|\delta u\| \leq \|M^{-1}\| \|v\|$  in any typical matrix norm. Since  $l_r, l_s \sim O(|t|^{n-3/2})$ , it is easily seen that  $\|v\| \sim O(|t|^{n-3/2})$  and from the leading order behaviors given in (A.3),  $\|M^{-1}\| \sim O(|t|^{-(n-1)})$ , which implies that  $\|\delta u\|$  is at most  $O(|t|^{-1/2})$ . Thus the approximate peak locations  $z_p^{(0)}$  and  $z_p^{min}$  are within  $O(|t|^{-1/2})$  for large  $|t|$ , which establishes the second assertion in (A.1).

In order to establish the first assertion in (A.1), we proceed in a similar way as above. Namely, we evaluate the partial derivatives  $G := u_{nr}$  and  $H := u_{ns}$  at  $z_p^{min}$  where  $F_{nr} = F_{ns} = 0$ . Indeed setting  $z = z_p$  in the linear approximation of  $G(z)$ ,  $H(z)$  near  $z = z_p^{min}$  and using the fact that  $G(z_p) = H(z_p) = 0$ , it is possible to obtain a linear system for  $\delta u = (\delta r, \delta s)^T$  with  $v = (G, H)(z_p^{min})$  and the coefficient matrix  $M$  which has entries  $G_r, H_s, G_s = H_r$  evaluated at  $z = z_p^{min}$ . In order to find the dominant behavior of the entries of  $M$  for  $|t| \gg 0$  we actually evaluate them at  $z = z_p^{(0)}$  instead of  $z_p^{min}$ . The error due to this approximation only gives a lower order (in  $|t|$ ) correction term to the leading order estimate  $\delta u \sim O(|t|^{-1/2})$  obtained this way. We do not include the detailed asymptotic expressions since they are straightforward but cumbersome.

## References

- [1] M. Ablowitz and H. Segur, *Solitons and the inverse scattering transform* (SIAM, Philadelphia, 1981).
- [2] M. Ablowitz and P. Clarkson, *Solitons, nonlinear evolution equations and inverse scattering* (Cambridge University Press, London, 1991).
- [3] M. J. Ablowitz and J. Villarroel, Solutions to the time dependent Schrödinger and the Kadomtsev-Petviashvili equations, *Phys. Rev. Lett.* **78** (1997) 570–573.
- [4] M. J. Ablowitz, S. Chakravarty, A. D. Trubatch, and J. Villarroel, A novel class of solutions of the non-stationary Schrödinger and the Kadomtsev-Petviashvili I equations, *Phys. Lett. A* **267** (2000) 132–146.
- [5] M. J. Ablowitz and J. Villarroel, Initial value problems and solutions of the Kadomtsev-Petviashvili equations, Proc. NATO ARW on New Trends in integrability and partial solvability (Cadiz, Spain) (A. B. Shabat et al eds), NATO Science Series **132** (Kluwer 2004).
- [6] M. J. Ablowitz, *Nonlinear Dispersive Waves* (Cambridge University Press, Cambridge, UK 2011).

- [7] H. Aref, Integrable, chaotic, and turbulent vortex motion in two-dimensional flows, *Ann. Rev. Fluid Mech.* **15** (1983) 345–389.
- [8] F. Calogero, Solution of the one-dimensional  $N$ -body problems with quadratic and/or inversely quadratic pair potentials, *J. Math. Phys.* **12** (1971) 419–436.
- [9] F. Calogero, Motion of poles and zeros of special solutions of nonlinear and linear partial differential equations and related solvable many-body problems, *Il Nuovo Cimento* **43B** (1978) 177–228.
- [10] J-H Chang, Asymptotic analysis of multilump solutions of the Kadomtsev–Petviashvili-I equation, *Theor. Mat. Phys.* **195** (2018) 676–689.
- [11] D. V. Chudnovsky and G. V. Chudnovsky, Pole expansions of nonlinear partial differential equations, *Il Nuovo Cimento*, **40B** (1977) 339–353.
- [12] G. Csordas, W. Smith and R. S. Varga, Lehmer pairs of zeros, the de Bruijn-Newman constant  $\Lambda$ , and the Riemann hypothesis, *Constr. Approx.* **10** (1994), 107–129
- [13] P. Dubard, V.B. Matveev, Multi-rogue waves solutions to the focusing NLS equation and the KP-I equation, *Nat. Hazards. Earth. Syst. Sci.* **11** (2011) 667–672.
- [14] V. G. Dubrovsky, The construction of exact multiple pole solutions of some (2+1)–dimensional integrable nonlinear evolution equations via the  $\bar{\partial}$ -dressing method, *J. Phys. A: Math. Gen.* **32** (1999) 369–390.
- [15] A. S. Fokas and M. J. Ablowitz, On the inverse scattering of the time-dependent Schrödinger equation and the associated Kadomtsev-Petviashvili equations, *Stud. Appl. Math* **69** (1983) 211–228.
- [16] K. A. Gorshkov, D. E. Pelinovsky, and Yu. A. Stepanyants, Normal and anomalous scattering, formation and decay of bound states of two-dimensional solitons described by the Kadomtsev-Petviashvili equation, *JETP* **104** (1993) 2704–2720.
- [17] R. Hirota, *The Direct Method in Soliton Theory* (Cambridge University Press, Cambridge, 2004).
- [18] E. Infeld and G. Rowlands, *Nonlinear waves, solitons and chaos*, 2<sup>nd</sup> ed. (Cambridge University Press, London, 2000).
- [19] R. S. Johnson and S. Thompson, A solution of the inverse scattering problem for the Kadomtsev-Petviashvili equation by the method of separation of variables, *Phys. Lett. A* **66** (1978) 279–281.
- [20] B. B. Kadomtsev and V. I. Petviashvili, On the stability of solitary waves in weakly dispersive media, *Sov. Phys. - Dokl.* **15** (1970) 539–541.
- [21] Y. Kodama, *Solitons in two-dimensional shallow water* (SIAM 2018).
- [22] I. Krichever, Rational solutions of the Kadomtsev-Petviashvili equation and integrable systems of  $n$  particles on a line, *Funct. Anal. Appl.* **12** (1978) 76–78.
- [23] K. E. Lonngren, Ion acoustic soliton experiments in a plasma, *Optical and Quantum Electronics* **30** (1998), 615–630.
- [24] S. V. Manakov, V. E. Zakharov, L. A. Bordag, A. R. Its and V. B. Matveev, Two-dimensional solitons of the Kadomtsev-Petviashvili equation and their interaction, *Phys. Lett. A* **63** (1977) 205–206.
- [25] V. Matveev, Some comments on the rational solutions of the Zakharov-Shabat equations, *Lett. Math. Phys.* **3** (1979) 503–512.
- [26] V. B. Matveev and M. A. Salle, *Darboux Transformations and Solitons* (Springer-Verlag, Berlin 1991).

- [27] S. P. Novikov, S. V. Manakov, L. P. Pitaevskii, and V. E. Zakharov, *Theory of Solitons. The Inverse Scattering Transform* (Plenum, New York, 1984).
- [28] Y. Ohta, J. Satsuma, D. Takahashi and T. Tokihiro, An elementary introduction to Sato theory, *Prog. Theor. Phys. Suppl.* **94** (1988) 210–241.
- [29] D. E. Pelinovskii and Yu. A. Stepanyants, New multisoliton solutions of the Kadomtsev-Petviashvili equation, *JETP Lett.* **57** (1993) 24–28.
- [30] D. Pelinovsky, Rational solutions of the Kadomtsev-Petviashvili hierarchy and the dynamics of their poles. I. New form of a general rational solution, *J. Math. Phys.* **35** (1994) 5820–5830.
- [31] D. Pelinovsky, Rational solutions of the KP hierarchy and the dynamics of their poles. II. Construction of the degenerate polynomial solutions, *J. Math. Phys.* **39** (1998) 5377–5395.
- [32] B. Rodgers and T. Tao, The de Bruijn-Newman constant is non-negative, *Forum of Mathematics, Pi* **8** e6 (2020), 62pp.
- [33] P. C. Rosenbloom and D. V. Widder, Expansions in terms of heat polynomials and associated functions, *Trans. Amer. Math. Soc.* **92** (1959), 220–266.
- [34] M. Sato, Soliton equations as dynamical systems on an infinite dimensional Grassmannian manifold, *RIMS Kokyuroku* (Kyoto University) **439** (1981) 30–46.
- [35] J. Satsuma and M. Ablowitz, Two-dimensional lumps in nonlinear dispersive systems, *J. Math. Phys.* **20** (1979) 1496–1503.
- [36] T. Shiota, Calogero-Moser hierarchy and KP hierarchy, *J. Math. Phys.* **35** (1994) 5844–5849.
- [37] T. J. Stieltjes, Sur quelques theoremes d’algebre, *Comptes Rendus* **100** (1885) 439–440.
- [38] T. J. Stieltjes, Sur les polynomes de Jacobi, *Comptes Rendus* **100** (1885) 620–622.
- [39] J. Villarroel and M. J. Ablowitz, On the discrete spectrum of the non-stationary Schrödinger equation, and multi-pole lumps of the Kadomtsev-Petviashvili I equation, *Commun. Math. Phys.* **207** (1999) 1–42.